Table 2. Characterization of PMBN/PLA Nanoparticles Prepared with Various Concentrations of PMBN[a]

PMBN (mg/mL)	diameter (nm)	ζ-potential (mV)
10.0	195	−5.3
1.0	204	−6.2
0.1	627	−6.7

[a] Preparation condition: PLA concentration 10 mg/mL. ζ-potential measurement was carried out in 10 mM NaCl aq. solution.

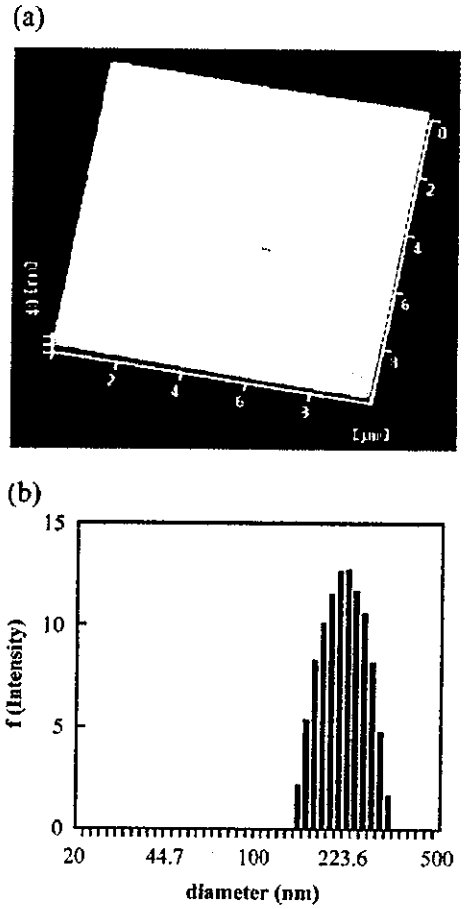

Figure 3. (a) AFM image of PMBN/PLA nanoparticles and (b) size distribution of PMBN/PLA nanoparticles prepared in 1.0 mg/mL PMBN.

The diameter of the PMBN/PLA nanoparticles was determined by DLS measurement. The diameter and ζ-potential was affected by the initial concentration of PMBN. When the initial concentration of PMBN was over the critical aggregate concentration from the fluorescence measurement of ANS (1.0 mg/mL), the diameter was 204 nm as the cumulant result in Marquadt analysis. In this case, the nanoparticles were stably dispersed in water. Figure 3 shows the AFM image (a) of the PMBN/PLA nanoparticles and the diameter histogram (b) from the DLS measurement.

This observation also indicated that the PMBN/PLA nanoparticles were spherical in shape and ca. 200 nm in diameter. The XPS charts of C1s, O1s, P2p, and N1s on the surface of the PMBN/PLA nanoparticles are shown in Figure 4. The PMBN/PLA nanoparticles had a phosphorus peak, a nitrogen peak, an oxygen peak, and a strong carbon peak

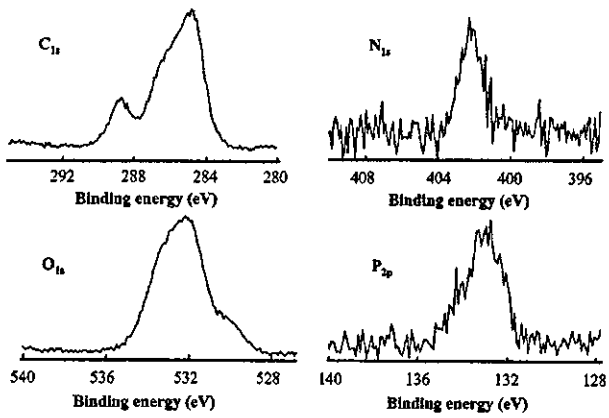

Figure 4. XPS charts of PMBN/PLA nanoparticles prepared in 1.0 mg/mL PMBN.

attributed to the methyl or methylene carbons. The surface of the PMBN/PLA nanoparticles was considered to be covered with phosphorylcholine groups in the MPC unit. Based on these results, it was indicated that the PMBN effectively acted as an emulsifier and a surface modifier due to its amphiphilic character.

To quantify the *p*-nitrophenyl ester groups on the nanoparticles, hydrolysis of the *p*-nitrophenyl ester bond in 0.01 M NaOH aqueous solution was carried out. The UV spectra of the *p*-nitrophenol released from the PMBN/PLA nanoparticles were detected, and the amount of active ester units on the PMBN/PLA nanoparticles was 7.6×10^{-9} mol/mg of nanoparticles.

An enzyme, ChO, was immobilized on the PMBN/PLA nanoparticles via condensation between the active ester groups and the amino groups of ChO. The immobilization reaction with the enzymes on the polymer nanoparticles induces release of *p*-nitrophenol with time. The obtained nanoparticles were called as ChO/PMBN/PLA nanoparticles. Un-conjugated ChO was removed completely from the nanoparticles by centrifugation. The schematic illustration of microdialysis sensor developed in this study was shown in Figure 5.

The obtained ChO/PMBN/PLA nanoparticles were filled into the microdialysis probe to create the enzymatic sensor. After addition of choline chloride as the substrate for ChO into the outer medium, the enzyme reaction occurred on the ChO/PMBN/PLA nanoparticles and produced hydrogen peroxide, which could be detected on the hydrogen peroxide electrode in the microdialysis probe [Figure 6a]. Figure 6b indicated an increase in current with the concentration of choline chloride in the outer solution. There was a good linear relationship between them; that is, the enzymatic reaction between immobilized ChO and the substrate choline chloride proceeded well.

Next, we carried out a dual-mode conjugation, which means immobilization of two kinds of enzymes on the same nanoparticle. As shown in Figure 7, when acetylcholine chloride was added in the outer solution, in which the microdialysis probe containing polymer nanoparticles was immersed, an increase in the current value could also be detected.

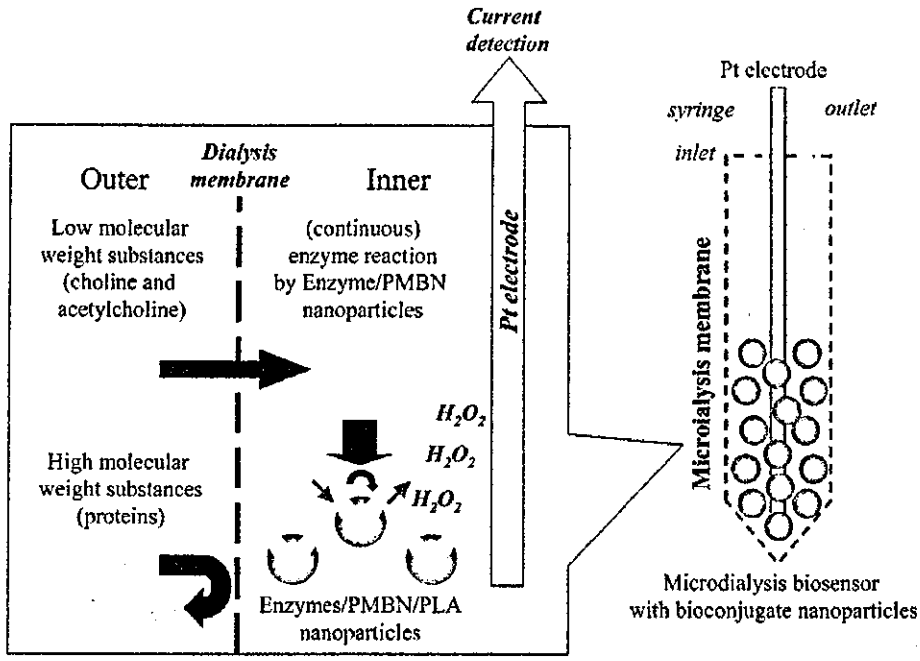

Figure 5. Schematic illustration of microdialysis biosensor system with bioconjugate nanoparticles.

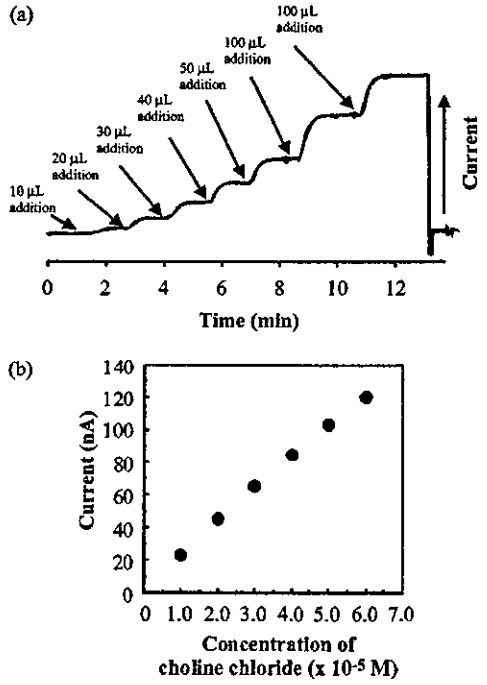

Figure 6. Enzymatic reaction of ChO on the surface of PMBN/PLA nanoparticles in the microdialysis probe, (a) the relationship between the change in the current value and the measurement time (outer medium was 50 mL; concentration of added choline chloride 1.5 mg/mL) and (b) the relationship between the concentration of added choline chloride and the current value.

Namely, the continuous enzymatic reaction could occur on the surface of polymer nanoparticles. As in the case of dual-mode conjugation of two kinds of enzymes, the local concentration of enzymes was higher, that is, the distance between AChE and ChO was small. Diffusion of the first product (choline) with AChE was easier and the choline was reacted with the second enzyme, ChO, as a second substrate. Therefore, the continuous enzyme reaction could occur smoothly. Based on these results, it was considered that the polymer nanoparticles could conjugate with specific biomolecules and these bioconjugated nanoparticles could be used in a diagnostic system. ACh is one of the most important neurotransmitters and is also believed to be involved in some severe diseases such as Alzheimer's, Parkinson's, epilepsy, and so on.[12,13] However, a real-time monitoring using a microdialysis system is difficult because the flow rate of the perfusion solution is quite slow. Therefore, the microdialysis system needs a long time to collect the analyte samples.[14,15] In this study, we confirmed that the continuous enzyme reactions occurred by dual-mode conjugation of two kinds of enzymes (ChO and AChE) on the polymer nanoparticles. From these findings, a novel diagnostic system can be prepared using the bioconjugated polymer nanoparticles covered with phosphorylcholine groups in the microdialysis probe.

Conclusion

A novel MPC polymer having *p*-nitrophenyl ester groups was designed and synthesized in this study. The MPC polymer had an amphiphilic character, and it could be used as an emulsifier and surface modifier for preparing polymer nanoparticles covered with phosphorylcholine groups and active ester groups. Two kinds of enzymes could be immobilized on the surface of the nanoparticles, and they could perform their specific function in the microdialysis probe. Continuous enzymatic reactions were realized on the polymer nanoparticles. That is, one substrate was added in the outer solution of the microdialysis probe containing polymer nanoparticles; it permeated through the hollow fiber and reacted with one enzyme on the polymer nanoparticles.

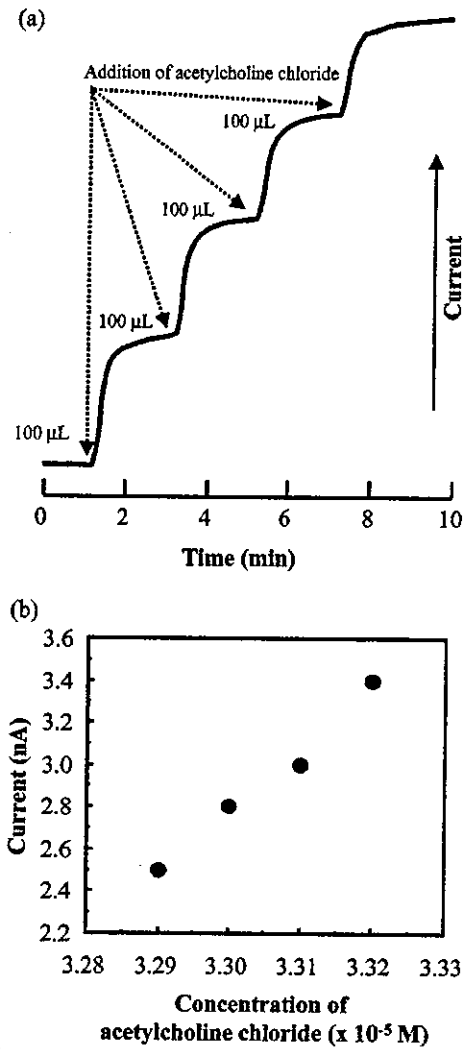

Figure 7. Continuous enzymatic reactions observed on the PMBN/PLA nanoparticles, (a) the relationship between the change in current value and measurement time (outer medium was 30 mL; concentration of acetylcholine chloride added in the solution was 1.5 mg/mL) and (b) the relationship between the concentration of added acetylcholine chloride and the height of the chart.

The product of the enzymatic reaction goes to the second enzyme as a substrate. The substrate is then reacted with the second enzyme. Increasing the local concentration of the enzymes and the adjacent effect of associated enzymes is considered to be important to increase the sensitivity of diagnostic agents. The combination of polymer nanoparticles conjugated with the enzymes and a microdialysis system with the electrode creates a new diagnostic system that can detect a target molecule in situ. That is, it does not need perfusion of a solution from the microdialysis probe for detection.

Acknowledgment. This study was partially supported by a Grant-in-Aid for Special Coordination Fund for Promoting Science and Technology. One of the authors (T.K.) was supported by a Grant for 21st century COE Program, "Human-Friendly Materials based on Chemistry" from the Ministry of Education, Culture, Sports, Science, and Technology of Japan.

References and Notes

(1) Konno, T.; Kurita, K.; Iwasaki, Y.; Ishihara, K. *Biomaterials* **2001**, *22*, 1883−1889.
(2) Ishihara, K.; Aragaki, R.; Ueda, T.; Watanabe, A.; Nakabayashi, N. *J. Biomed. Mater. Res.* **1990**, *24*, 1069−1077.
(3) Ishihara, K.; Oshida, H.; Ueda, T.; Endo, Y.; Watanabe, A.; Nakabayashi, N. *J. Biomed. Mater. Res.* **1992**, *26*, 1543−1552.
(4) Ishihara, K.; Iwasaki, Y.; Ebihara, S.; Shindo, Y.; Nakabayashi, N. *Colloid Surf. B: Biointerfaces* **2000**, *18*, 325−335.
(5) Ishihara, K.; Iwasaki, Y. *Polym. Adv. Technol.* **2000**, *11*, 626−634.
(6) Iwasaki, Y.; Nakabayashi, N.; Ishihara, K. *J. Biomed. Mater. Res.* **2001**, *57*, 74−79.
(7) Trubetskoy, V. S. *Adv. Drug. Delivery Rev.* **1999**, *37*, 81−88.
(8) Solovskij, M. V.; Panarin, E. F.; Gorbunova, O. P.; Korneeva, E. V.; Petuhkova, N. A.; Michajlova, N. A.; Pavlov, G. M. *Eur. Polym. J.* **2000**, *36*, 1127−1135.
(9) Torchilin, V. P.; Levchenko, T. S.; Lukyanov, A. N.; Khaw, B. A.; Kilbanov, A. L.; Rammohan, R.; Samokhin, G. P.; Whiteman, K. R. *Biochim. Biophy. Acta* **2001**, 1511, 397−411.
(10) Ishihara, K.; Ueda, T.; Nakabayashi, N. *Polym. J.* **1990**, *22*, 355−360.
(11) Ishihara, K.; Iwasaki, Y.; Nakabayashi, N. *Polym. J.* **1999**, *31*, 1231−1236.
(12) Fisher, A., Hanin, I., Lachman, C., Eds.; *Alzheimer's and Parkinson's Diseases: Strategies for Research and Development*; Plenum Press: New York, 1986.
(13) Larsson, N.; Ruzgas, T.; Gorton, L.; Kokaia, M.; Kissinger, P.; Csöregi, E. *Electrochim. Acta* **1998**, *43*, 3541−3554.
(14) Davies, M. I.; Cooper, J. D.; Desmond, S. S.; Lunte, C. E.; Lunte, S. M. *Adv. Drug. Delivery Rev.* **2000**, *45*, 169−188.
(15) Torto, N.; Laurell, T.; Gorton, L.; Varga, G. M. *Anal. Chim. Acta* **1999**, *379*, 281−305.

BM034356P

MOLECULAR AND CELLULAR BIOLOGY, Aug. 2004, p. 6560–6568 Vol. 24, No. 15
0270-7306/04/$08.00+0 DOI: 10.1128/MCB.24.15.6560–6568.2004

Bone Morphogenetic Protein 2-Induced Osteoblast Differentiation Requires Smad-Mediated Down-Regulation of Cdk6

Toru Ogasawara,[1,2] Hiroshi Kawaguchi,[2] Shigeki Jinno,[1] Kazuto Hoshi,[2] Keiji Itaka,[2] Tsuyoshi Takato,[2] Kozo Nakamura,[2] and Hiroto Okayama[1]*

Departments of Biochemistry and Molecular Biology[1] and Sensory and Motor System Medicine,[2] The University of Tokyo Graduate School of Medicine, Tokyo 113-0033, Japan

Received 31 March 2004/Accepted 8 May 2004

Because a temporal arrest in the G_1 phase of the cell cycle is thought to be a prerequisite for cell differentiation, we investigated cell cycle factors that critically influence the differentiation of mouse osteoblastic MC3T3-E1 cells induced by bone morphogenetic protein 2 (BMP-2), a potent inducer of osteoblast differentiation. Of the G_1 cell cycle factors examined, the expression of cyclin-dependent kinase 6 (Cdk6) was found to be strongly down-regulated by BMP-2/Smads signaling, mainly via transcriptional repression. The enforced expression of Cdk6 blocked BMP-2-induced osteoblast differentiation to various degrees, depending on the level of its overexpression. However, neither BMP-2 treatment nor Cdk6 overexpression significantly affected cell proliferation, suggesting that the inhibitory effect of Cdk6 on cell differentiation was exerted by a mechanism that is largely independent of its cell cycle regulation. These results indicate that Cdk6 is a critical regulator of BMP-2-induced osteoblast differentiation and that its Smads-mediated down-regulation is essential for efficient osteoblast differentiation.

Bone morphogenetic protein 2 (BMP-2) is a potent inducer of bone formation through its stimulation of osteoblast differentiation (17). It exerts this effect via two types of serine/threonine kinase receptors: BMP-2 binds the type II receptor, which subsequently activates the type I receptor by a direct association. Signals from the activated type I receptor are transmitted to the nucleus through various mediator molecules, the most important among them being a family of proteins termed Smads. Smads are classified into three subgroups, i.e., Smad1, Smad5, and Smad8 are classified as receptor-regulated Smads (R-Smads), Smad4 is classified as a common-partner Smad (Co-Smad), and Smad6 and Smad7 are classified as inhibitory Smads (I-Smads) (6). R-Smads are directly activated by the type I receptor, form complexes with Co-Smad, and are translocated into the nucleus, where they regulate the transcription of target genes. I-Smads inhibit the activation of R-Smads by interfering with their association with the type I receptor, which results in the hindrance of the assembly of R-Smads with Co-Smad. Although the downstream signaling of the BMP-2/Smad pathway leading to osteoblast differentiation has been extensively investigated, most of the studies have focused on the bone-related transcriptional regulators Runx2/Cbfa1 (7, 31), osterix (12), SIP1 (25), Smurf1 (32), NF-κB (4, 9), Hoxc-8 (1, 20), and Tob (29).

The proliferation of eukaryotic cells depends on their progression through the cell cycle, and an at least temporal cell cycle arrest in the G_1 phase is thought to be a prerequisite for cell differentiation (18). Cell cycle progression is controlled by the action of cyclins and cyclin-dependent protein kinases (Cdks), which phosphorylate and thereby activate cell cycle factors that are essential for the onset of the next cell cycle phase. In mammalian cells, traverse through G_1 and subsequent S-phase entry require the activities of the cyclin D-dependent kinase Cdk4 and/or Cdk6 (11) and the cyclin E-dependent kinase Cdk2. A key physiological substrate for Cdk4 and Cdk6 is the retinoblastoma (Rb) protein, which binds and inactivates the E2F-DP transcription complexes that are essential for S-phase entry. Phosphorylation by Cdk4/6 and additionally by Cdk2 inactivates Rb, thereby releasing E2F-DP from inactivation and consequently promoting S-phase entry and progression (5, 14). These Cdks are negatively regulated by cyclin-dependent kinase inhibitors (CKIs) via direct binding to themselves (19, 26). CKIs have been classified into two families, the INK4 family and the Cip/Kip family. INK4 family members (p16, p15, p18, and p19) inhibit only Cdk4 and Cdk6, whereas Cip/Kip family members (p21, p27, and p57) inhibit all of the Cdks except for the Cdk6-cyclin D3 complex. Because of its unique ability to evade inhibition by Cip/Kip proteins, Cdk6-D3 can control the cell's proliferative potential under growth-suppressive conditions despite its relative minority in level of expression in mesenchymal cells (8).

Cdks play crucial roles in controlling cell cycle progression. Therefore, much attention has been attracted by the view that the CKI-led inhibition of G_1-specific Cdks is critical for cell differentiation. Accordingly, potential roles for CKIs in differentiation have been extensively studied, but with mixed results. Many studies revealed a certain correlation between the induction of $p21^{CIP1}$ and differentiation, yet many did not. Mice with a complete deletion of $p21^{CIP1}$ and/or $p27^{KIP1}$ or other major CKIs still develop normally, with proper differentiation, which calls the current view into question (3, 13). Although there is evidence for $p57^{KIP2}$ being involved in the differentiation of some cells (28, 30), no one has identified cell cycle factors that are controlled by differentiation signals and that critically influence the differentiation commitment process.

* Corresponding author. Mailing address: Department of Biochemistry and Molecular Biology, Graduate School and Faculty of Medicine, University of Tokyo, 7-3-1 Hongo, Bunkyo, Tokyo 113-0033, Japan. Phone: 81-3-5841-3440. Fax: 81-3-3815-1490. E-mail: okayama-tky@umin.ac.jp.

Since in lower eukaryotes the control of the cell cycle factors driving the onset of S phase greatly influences the commitment to cell differentiation, we reinvestigated the possibility of the crucial participation of some cell cycle start factors in mammalian cell differentiation control as well, using BMP-2-induced osteoblast differentiation as a model system, and we found that upon BMP-2 treatment, Cdk6 expression was down-regulated primarily by BMP-2/Smad signal-invoked transcriptional repression and that its down-regulation was essential for efficient osteoblast differentiation.

MATERIALS AND METHODS

Reagents and antibodies. Recombinant human BMP-2 was generously provided by Yamanouchi Pharmaceutical Co., Ltd. (Tokyo, Japan), and recombinant human fibroblast growth factor 2 (FGF-2) was provided by Kaken Pharmaceutical Co., Ltd. (Chiba, Japan). Antibodies against Cdk2 (H-298), Cdk4 (C-22), Cdk6 (C-21), Rb (C-15), cyclin D1 (C-20), cyclin D2 (M-20), cyclin D3 (C-16), cyclin E (M-20), p18 (M-20), p21 (H164), p27 (F-8), BMPRIA (E-16), BMPRII (T-18), and Smad6 (S-20) were obtained from Santa Cruz Biotechnology. Anti-phosphorylated Rb (G3-245) and anti-β-actin (AC-15) antibodies were purchased from Pharmingen and Sigma, respectively.

Osteoblast culture. The mouse osteoblast cell line MC3T3-E1 was purchased from the Riken Cell Bank (Tsukuba, Japan). Primary osteoblasts were isolated from neonatal mouse calvariae according to international and university guidelines (33). Calvariae dissected from 1- to 4-day-old mice were digested for 10 min with 1 ml of trypsin-EDTA (Sigma) containing 10 mg of collagenase (type 7; Sigma), and the released cells were collected. This step was repeated five times, and the cells obtained by the second through fifth digestion steps were pooled as primary osteoblasts. MC3T3-E1 cells and primary osteoblasts were maintained in α-modified minimum essential medium (α-MEM) (Life Technologies Inc.) containing 10% fetal bovine serum (FBS) (Sigma). The cells were inoculated at 5×10^4 cells in a six-well plate or 5×10^5 cells in a 10-cm-diameter plate and allowed to proliferate for 20 to 24 h, and then their growth was arrested by incubation for 24 to 48 h in α-MEM containing 0.5% FBS. Growth-arrested cells were then induced for differentiation or proliferation by stimulation with α-MEM containing 10% FBS and BMP-2 (300 ng/ml) or FGF-2 (10 nM). To block protein degradation, we added the proteasome inhibitor MG132 (Z-Leu-Leu-Leu-aldehyde; Peptide Institute, Osaka, Japan) to the culture medium to a final concentration of 2 μM, as described previously (15, 24).

Construction of cell clones constitutively expressing Cdk6. MC3T3-E1 cells were inoculated at 5×10^5 cells per 6-cm-diameter plate, incubated for 24 h, and then transfected with the pEF/neo I vector carrying a human *Cdk6* cDNA or no insert by use of the Lipofectamine reagent (Life Technologies, Inc.) according to the manufacturer's instructions. Twenty-four hours later, the cells were split 1:10 to 1:100 and selected in α-MEM containing 10% FBS and 200 μg of G418 (Geneticin; Life Technologies, Inc.)/ml. Stable G418-resistant colonies were then isolated and expanded for analysis. The levels of Cdk6 were then quantified by Western blotting to identify several high- and low-expression-level clones for in-depth analysis.

Smad6 expression and differentiation induction. MC3T3-E1 cells were inoculated at 5×10^4 cells per well in a six-well plate and incubated at 37°C for 20 h in α-MEM containing 10% FBS. The cells were then infected for 2 h with a recombinant adenovirus carrying *smad6* or *lacZ* at a multiplicity of infection of 100 PFU/cell, for which >80% of the cells were infected, as determined by staining for β-galactosidase. The cells were washed twice with phosphate-buffered saline (PBS), their growth was arrested by incubation in α-MEM containing 0.5% FBS for 48 h, and they were stimulated with α-MEM containing 10% FBS with or without BMP-2 (300 ng/ml).

Western blot analysis. The cells were rinsed with ice-cold PBS and lysed with RIPA buffer (10 mM Tris-HCl [pH 7.5], 150 mM NaCl, 1% Nonidet P-40 [NP-40], 0.1% sodium dodecyl sulfate [SDS], 10 μg of aprotinin/ml, 0.1 M NaF, 2 mM Na_3VO_4, and 10 mM β-glycerophosphate). After a brief sonication, the lysed cells were centrifuged at 15,000 × *g* for 20 min at 4°C to obtain soluble cell extracts. The cell extracts (10 μg of protein each) were separated by SDS–7.5, 10, or 12.5% polyacrylamide gel electrophoresis and electrotransferred to polyvinylidene difluoride membranes (Immobilon-P; Millipore Corp., Bedford, Mass.). After the blocking of nonspecific binding by soaking of the filters in 5% skim milk, the desired proteins were immunodetected with their respective antibodies, followed by visualization by use of the ECL Plus Western blotting detection system (Amersham Pharmacia Biotech, Buckinghamshire, United Kingdom) according to the manufacturer's instructions.

In vitro kinase assay. Cells were lysed with ice-cold IP buffer containing 50 mM HEPES (pH 7.5), 150 mM NaCl, 1 mM EDTA, 2.5 mM EGTA, 1 mM dithiothreitol, 0.1% Tween 20, 10% glycerol, 1 mM phenylmethylsulfonyl fluoride (PMSF), 10 μg of aprotinin/ml, 1 mM NaF, and 0.1 mM sodium orthovanadate. The lysates were incubated at 4°C for 2 h with 0.5 μg of the anti-Cdk4 or -Cdk6 antibody. Protein G-Sepharose (15 μl) (Amersham-Pharmacia) was then added and incubated for an additional 1 h. Immune complexes bound to protein G-Sepharose were precipitated by centrifugation and washed with glycerol-free IP buffer. The immunopurified Cdk4 or Cdk6 protein was incubated at 30°C for 30 min in R buffer (50 mM HEPES [pH 7.5], 2.5 mM EGTA, 10 mM KCl, 10 mM $MgCl_2$, 1 mM dithiothreitol) containing 0.5 μg of truncated Rb (Santa Cruz) and 10 mM ATP. The reaction products were electrophoresed in SDS–10% polyacrylamide gels and transferred to polyvinylidene difluoride membrane filters. Phosphorylated truncated Rb was detected with an anti-Ser780-phosphorylated Rb antibody (MBL).

Reverse transcription-PCR (RT-PCR). Total RNAs (1 μg) extracted from cells were reverse transcribed and amplified by PCR. The gene-specific primer pairs used were as follows: 5′-CGTGGTCAGGTTGTTTGATG-3′ and 5′-TGCGAAACATTTCTGCAAAG-3′ for Cdk6, 5′-ATGAGGACCCTCTCTCTGCT-3′ and 5′-CCGTAGATGCGTTTGTAGGC-3′ for osteocalcin, 5′-TAGCACCAGAGGATACCTTGC-3′ and 5′-AATGCTTCATCCTGTTCCAAA-3′ for BMPRIA, 5′-CAGAATCAAGAACGGCTATG-3′ and 5′-TTGTTTACGGTCTCCTGTCA-3′ for BMPRII, and 5′-CATGTAGGCCATGAGGTCCACCAC-3′ and 5′-TGAAGGTCGGTGTGAACGGATTTGGC-3′ for glyceraldehyde-3-phosphate dehydrogenase. The cycling parameters were 30 s at 94°C, 30 s at 55°C, and 1 min 30 s at 72°C for Cdk6, osteocalcin, and glyceraldehyde-3-phosphate dehydrogenase; and 30 s at 94°C, 30 s at 53°C, and 1 min 30 s at 72°C for BMPRIA and BMPRII.

ALP activity measurement and in situ staining. MC3T3-E1 cells were inoculated at 5×10^4 cells per well in a six-well plate and cultured in α-MEM containing 10% FBS with or without BMP-2 (300 ng/ml). After being cultured for 3 days, the cells were rinsed with PBS and lysed by sonication in 10 mM Tris-HCl buffer (pH 8.0) containing 1 mM $MgCl_2$ and 0.5% Triton X-100. The alkaline phosphatase (ALP) activity in the lysates was measured by the hydrolysis of *p*-nitrophenyl phosphate to *p*-nitrophenol. The protein content was determined by using a protein assay kit (Bio-Rad). For in situ ALP staining, the cells were fixed with 3.7% (vol/vol) formaldehyde in PBS and were stained with naphthol AS-MX phosphate (Sigma), with *N,N*-dimethyl formamide as a substrate and Fast BB salt (Sigma) as a coupler.

BrdU incorporation assay. MC3T3-E1 cells were inoculated at 10^3 cells per well in a 96-well plate and cultured in α-MEM containing 10% FBS with or without BMP-2 (300 ng/ml). After being cultured for 1 or 3 days, the cells were labeled with bromodeoxyuridine (BrdU) for 2 h, and the cell population entering S phase was determined by quantifying the incorporated BrdU (Cell Proliferation ELISA; Roche Molecular Biochemical, Mannheim, Germany).

XTT assay. Cells were inoculated at 10^3 cells per well in a 96-well plate and cultured for 5 days in α-MEM containing 10% FBS with or without BMP-2 (300 ng/ml), with cell sampling every day. The sampled cells were quantified by use of an XTT {sodium 3,3-[(phenylamino)carbonyl]-3,4-tetrazolium-bis(4-methoxy-6-nitro) benzenesulfonic acid hydrate} assay kit (Roche).

Flow cytometric analysis. Approximately 10^5 cells were suspended in 0.02 ml of citrate buffer and subjected to the following serial treatments at room temperature: (i) the addition of 0.18 ml of solution A (0.03 mg of trypsin/ml, 3.4 mM trisodium citrate, 0.1% NP-40, 1.5 mM spermine 4HCl, and 0.5 mM Tris-HCl [pH 7.6]) and incubation for 10 min; (ii) the addition of 0.15 ml of solution B (3.4 mM trisodium citrate, 0.1% NP-40, 1.5 mM spermine-4HCl, 0.5 mM Tris-HCl [pH 7.6], 0.5 mg of trypsin inhibitor/ml, 0.1 mg of RNase A/ml) and incubation for 10 min; and (iii) the addition of 0.15 ml of solution C (4.16 mg of propidium iodide/ml, 3.4 mM trisodium citrate, 0.1% NP-40, 4.8 mM spermine 4HCl, 0.5 mM Tris-HCl [pH 7.6]) and incubation for 10 min. The DNA content was determined and analyzed with EPICS XL and XL EXPO32 instruments (Beckman).

ChIP. Chromatin immunoprecipitation (ChIP) was performed by use of a commercial kit (Upstate Cell Signaling Solutions, Lake Placid, N.Y.). Cells were inoculated at a density of 5×10^5 cells per 10-cm-diameter dish and cultured in α-MEM containing 10% FBS and BMP-2 (300 ng/ml). At days 1 and 4 of culture, the protein and DNA were cross-linked by the direct addition of formaldehyde to the culture medium to a final concentration of 1% and incubation at 37°C for 10 min. The cells were then washed twice with ice-cold PBS containing 1 mM PMSF and 1 μg of aprotinin/ml, collected with cell scrapers, sedimented by low-speed centrifugation, resuspended, and incubated at 4°C for 10 min in 200 μl

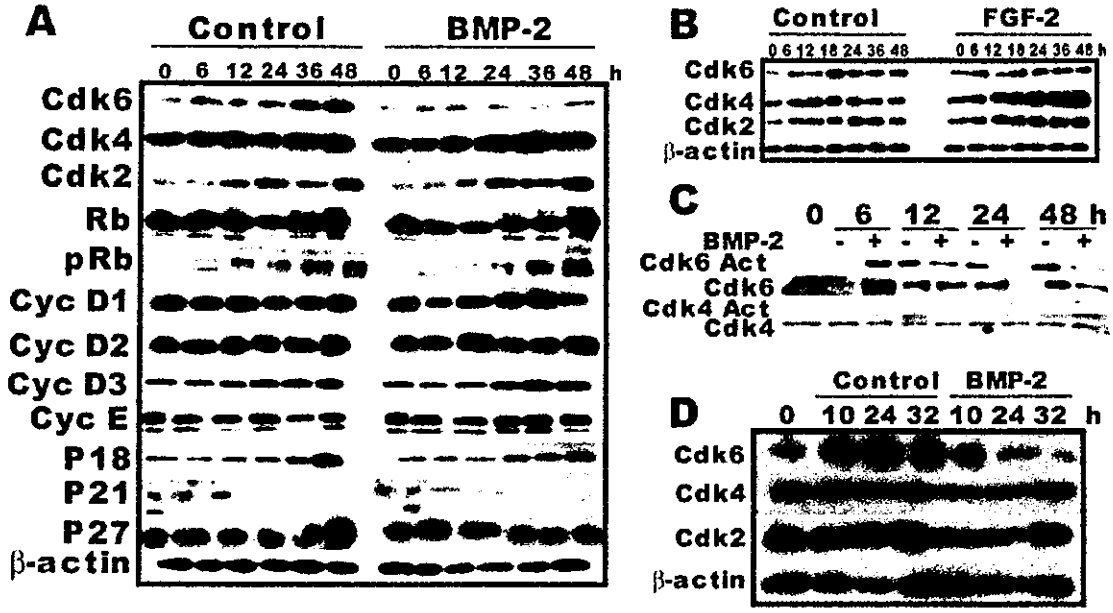

FIG. 1. BMP-2 treatment inhibits expression of Cdk6. (A) Time-dependent expression of cell cycle factors controlling the G_1-S transition in mouse osteoblastic MC3T3-E1 cells during differentiation induction. Growth-arrested MC3T3-E1 cells were stimulated with FBS in the presence or absence of BMP-2, with cell sampling done at the indicated times. The amounts of cell cycle factors expressed during stimulation were semiquantified by Western blotting. β-Actin was used as a loading control. Cyc, cyclin. (B) Time-dependent expression of Cdks 2, 4, and 6 in MC3T3-E1 cells during FGF-2 stimulation. Growth-arrested MC3T3-E1 cells were stimulated with FBS in the presence or absence of FGF-2, with cell sampling performed at the indicated times, followed by Western blotting of Cdks 2, 4, and 6. (C) Cdk6 and Cdk4 activities in MC3T3-E1 cells during stimulation with or without BMP-2. Cdk6 and Cdk4 were immunoprecipitated and assayed for kinase activity, and their amounts were determined in parallel. (D) Time-dependent expression of Cdk2, Cdk4, and Cdk6 proteins in primary neonatal mouse calvarial osteoblasts stimulated with or without BMP-2.

of lysis buffer (1% SDS, 10 mM EDTA, 50 mM Tris [pH 8.1]) containing 1 mM PMSF and 1 μg of aprotinin/ml. The cell lysates were then sonicated at 4°C with a Branson 450 sonifier at an output control of 2 and a duty cycle of 10 for 10 s to fragment the chromosomal DNA into 0.2- to 1-kb pieces. After the insoluble material was removed by centrifugation at 15,000 × *g* for 10 min, 1/10 aliquots of the supernatants were taken and saved as input. The rest of the supernatants were diluted appropriately with ChIP dilution buffer (0.01% SDS, 1.1% Triton X-100, 1.2 mM EDTA, 16.7 mM Tris-HCl [pH 8.1], 167 mM NaCl) containing 1 mM PMSF and 1 μg of aprotinin/ml and were pretreated with a salmon sperm DNA–protein A–50% agarose slurry at 4°C for 30 min with gentle agitation. After a brief centrifugation to remove the slurry, the supernatants were collected and incubated at 4°C overnight with antibodies (anti-mouse pRb [1 μg each of Ab-4 and Ab-5; Neomarkers] or anti-CBFA1 [2 μg of sc-8566; Santa Cruz]). Immunocomplexes were allowed to bind to protein A-agarose by incubation with a salmon sperm DNA–protein A–50% agarose slurry at 4°C for 1 h with gentle agitation. After a brief centrifugation, the supernatants were saved as the unbound fraction. The protein A-bound immunocomplexes were washed once with 1 ml each of the buffers shown below in sequential order: (i) low-salt immune complex wash buffer (0.1% SDS, 1% Triton X-100, 2 mM EDTA, 20 mM Tris-HCl [pH 8.1], 150 mM NaCl), (ii) high-salt immune complex wash buffer (0.1% SDS, 1% Triton X-100, 2 mM EDTA, 20 mM Tris-HCl [pH 8.1], 500 mM NaCl), (iii) LiCl immune complex wash buffer (0.25 M LiCl, 1% IGEPAL-CA630, 1% sodium deoxycholate, 1 mM EDTA, 10 mM Tris, pH 8.1), and (iv) TE buffer (10 mM Tris-HCl, 1 mM EDTA, pH 8.0). The protein A-bound immunocomplexes were resuspended in 250 μl of elution buffer (1% SDS, 0.1 M $NaHCO_3$), mixed by vortexing, and incubated at room temperature for 15 min, with gentle agitation. After a brief centrifugation, the supernatants were saved, and elution was repeated one more time. Both eluates were combined, and after the addition of 20 μl of 5 M NaCl, were heated at 65°C for 4 h to reverse cross-linking. Ten microliters of 0.5 M EDTA, 20 μl of 1 M Tris-HCl (pH 6.5), and 2 μl of proteinase K (20 mg/ml) were added to the eluates, and the mixtures were incubated for 1 h at 45°C to remove proteins bound to DNA, followed by sequential extraction steps with phenol-chloroform and chloroform and by DNA precipitation with ethanol after the addition of 10 μg of glycogen as a carrier. The precipitated DNA was recovered by centrifugation and resuspended in 100 μl of TE buffer. The input fractions of the supernatants and the unbound fractions were similarly treated to remove cross-links and proteins, and the DNAs were ethanol precipitated similarly and dissolved in 10 and 100 μl of TE buffer, respectively. The osteocalcin and myogenin promoter sequences were amplified by 40 cycles of PCR from 1 μl each of the DNA solutions, with parameters of 30 s at 95°C, 30 s at 60°C, and 30 s at 72°C and with the following primers: 5′-CTGAACTGGGCAAATGAGGACA-3′ and 5′-AGGGGATGCT GCCAGGACTAAT for the mouse osteocalcin promoter (positions −67 to −471) and 5′-ACCCCTTTCTTGTTCCCTTCCT-3′ and 5′-CTCCCGCAGCC CCTCAC-3′ for the mouse myogenin promoter (positions −9 to −431).

Statistical analysis. The means of groups were compared by analysis of variance, and the significance of differences was determined by post hoc testing using the Bonferroni method.

RESULTS

Cdk6 is down-regulated in osteoblasts upon BMP-2 treatment. Within 24 h after treatment with BMP-2, C2C12 cells begin to express osteocalcin mRNA and ALP, two representative markers of mature osteoblasts (21). Accordingly, the commitment to BMP-2-induced osteoblast differentiation occurs within 24 h. Since the MC3T3-E1 cells used in the present study are known to be in a stage that is one step more differentiated toward mature osteoblasts than C2C12 cells, we assumed that the commitment of this cell line to BMP-2-induced osteoblast differentiation occurred well within 24 h, and therefore we analyzed the effect of BMP-2 on the initial 48-h expression levels of cell cycle factors that critically regulate the onset of S phase in this cell line. The cells were arrested in quiescence by serum starvation, stimulated with serum in the presence or absence of BMP-2, and harvested every 6 or 12 h. The amounts of cyclins (D1, D2, D3, and E), Cdk2, Cdk4,

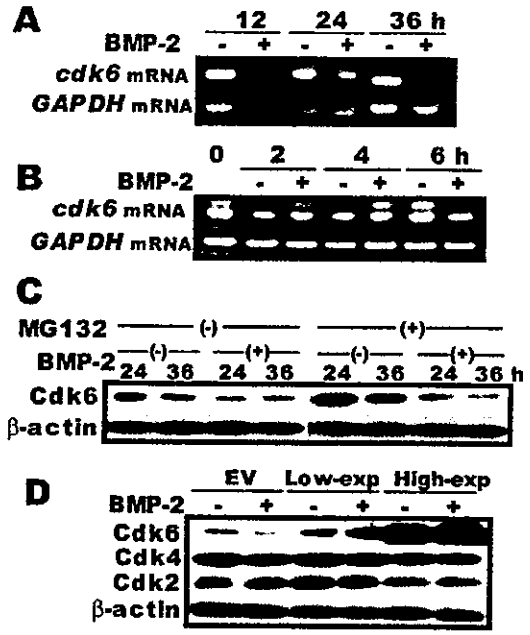

FIG. 2. BMP-2 down-regulates Cdk6 expression mainly via preventing transcription. (A) BMP-2 treatment markedly reduces *cdk6* mRNA level. Growth-arrested MC3T3-E1 cells were stimulated with or without BMP-2 for the indicated times, and RNAs were prepared. *cdk6* mRNA was semiquantified by RT-PCR. (B) BMP-2 treatment does not affect the stability of *cdk6* mRNA. Growth-arrested MC3T3-E1 cells were stimulated with serum for 6 h and then incubated with actinomycin D (Sigma) (0.1 μg/ml) with or without the addition of BMP-2. RNAs were prepared and the Cdk6 transcript was semiquantified by RT-PCR. Glyceraldehyde-3-phosphate dehydrogenase (GAPDH) mRNA was used as a control for the RNA preparations. (C) The proteasome inhibitor MG132 does not influence the action of BMP-2 on the Cdk6 protein level. Growth-arrested MC3T3-E1 cells were stimulated for 24 and 36 h with or without BMP-2 and/or MG132 (2 μM), and the Cdk6 protein levels were determined by Western blotting. (D) BMP-2 treatment does not affect the level of forcefully expressed Cdk6 protein. Clones constitutively expressing Cdk6 from an EF1α-promoter as well as empty vector-transfected MC3T3-E1 (EV) cells were growth arrested as described in the text and stimulated for 48 h with or without BMP-2. The amounts of Cdk6, Cdk4, and Cdk2 were then semiquantified by Western blotting.

Cdk6, CKIs (p18, p21, p27, and p57), and Rb and phosphorylated Rb proteins in the whole-cell lysate at each time point were analyzed by Western blotting (Fig. 1). In this cell line, the amounts of Cdk6, Cdk2, and p18 increased during serum stimulation, as early as 6 h after stimulation, and the amount of p21 decreased, whereas the amounts of the remaining factors were unchanged. This cell line did not express detectable amounts of p57 throughout the experiment (data not shown). Coinciding with the elevation of Cdk2, phosphorylated forms of the Rb protein appeared. Under these conditions, the cells grew to confluence but did not commit to differentiation into osteoblasts.

In contrast, when MC3T3-E1 cells were stimulated with BMP-2 to stimulate osteoblast differentiation, the induction of Cdk6 completely disappeared (Fig. 1A), while the levels of the remaining factors, including Cdk4, were virtually indistinguishable from those obtained by serum stimulation. The behavioral difference between Cdk6 and Cdk4 was further noticeable in another experiment. When MC3T3-E1 cells were treated with FGF-2, a potent stimulator of osteoblast proliferation, the level of Cdk4, but not that of Cdk6, was markedly elevated (Fig. 1B).

To confirm that the blocked induction of Cdk6 was faithfully reflected by its kinase activities, we assayed the activities of Cdk6 and Cdk4 during serum stimulation in the presence and absence of BMP-2. When the cells were stimulated with serum, Cdk6 activity increased at 12 h and remained high at least until 48 h. In contrast, when the cells were stimulated with serum containing BMP-2, Cdk6 activity increased at 6 h, but rapidly decreased to the basal level by 12 and 24 h, the times expected for the commitment to differentiation to take place (Fig. 1C). These activities were roughly correlated with the amounts of immunoprecipitated Cdk6, which faithfully reflected its amounts in whole-cell lysates (Fig. 1A), except for the BMP-2-treated 6-h sample, from which Cdk6 was more efficiently immunoprecipitated. This result was reproducible, but its reason was unclear.

On the other hand, there was no significant difference in the time course and extent of Cdk4 activation between BMP-2-treated and untreated MC3T3-E1 cells. Thus, despite the fact that Cdk4 and Cdk6 are structurally homologous (11) and share D cyclins as their catalytic partners, only the expression of Cdk6 was significantly influenced by BMP-2 treatment. We did a similar experiment with proliferating MC3T3-E1 cells and observed a similar down-regulation of Cdk6 upon BMP-2 treatment, although it was less obvious, perhaps due to the lack of synchronization in their cell cycle progression (data not shown).

Cdk6 down-regulation is not specific to this cell line and is a more general phenomenon. We performed the same Western blot analysis with a culture of primary osteoblasts isolated from neonatal mouse calvariae and obtained the same results. Treatment with BMP-2 during serum stimulation completely blocked the induction of Cdk6 at 24 and 32 h, whereas Cdk4 and Cdk2 were uninfluenced (Fig. 1D). These results show that Cdk6 was specifically down-regulated during the commitment to BMP-2-induced osteoblast differentiation.

BMP-2-led Cdk6 down-regulation is exerted at the transcriptional level. We performed a semiquantitative RT-PCR analysis of the Cdk6 transcript and found that *cdk6* mRNA disappeared when MC3T3-E1 cells were stimulated with BMP-2 (Fig. 2A). In contrast, BMP-2 did not significantly influence the stability of either *cdk6* mRNA or protein. When the cells were stimulated with serum for 6 h and then treated with

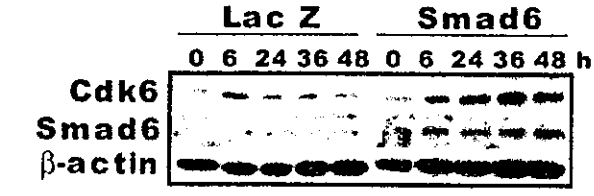

FIG. 3. Smad6 overexpression effectively blocks BMP-2-led down-regulation of Cdk6. MC3T3-E1 cells were infected with a recombinant adenovirus carrying the *smad6* or *lacZ* gene and were subsequently growth arrested by incubation in a low-serum-level medium for 48 h. The cells were then stimulated with serum in the presence or absence of BMP-2. The expression of Cdk6 and Smad6 was determined by Western blotting, with β-actin used as a loading control.

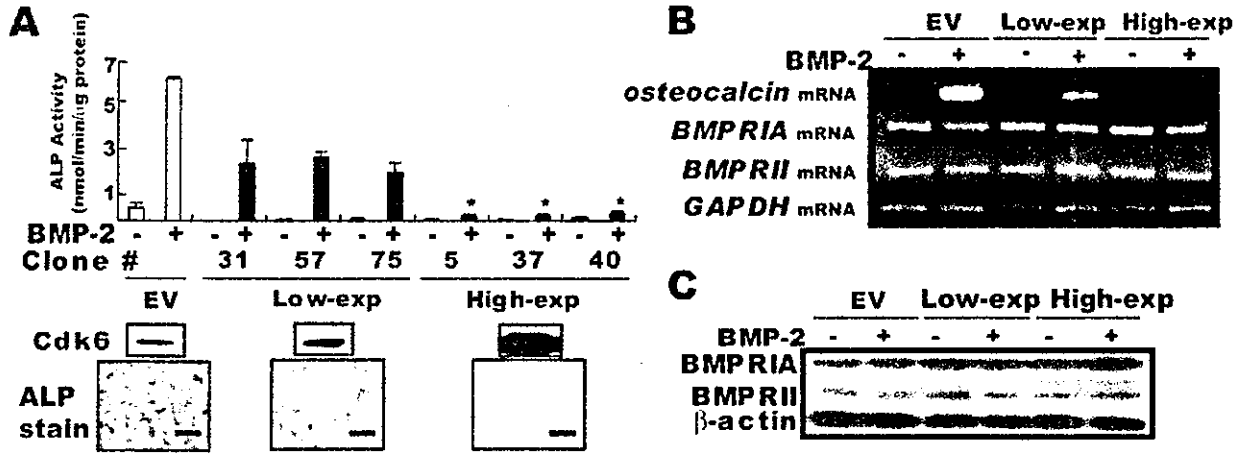

FIG. 4. Overexpression of Cdk6 inhibits BMP-2-induced osteoblast differentiation. MC3T3-E1 cell clones expressing low (no. 31, 57, and 75) or high (no. 5, 37, and 40) levels of Cdk6 and empty vector-transfected MC3T3-E1 (EV) cells were induced for osteoblast differentiation by treatment with BMP-2 according to the standard protocol. (A) After 72 h of treatment, the induced ALP activity was assayed (top). The middle panel shows Western blot data for Cdk6 in growing empty vector-transfected cells and cells from clones 31 and 40. *, $P < 0.1$; there is a significant difference from the ALP activity of BMP-2-treated empty vector-transfected cells. The bottom panels show ALP staining of empty vector-transfected cells and clones 31 and 40. Bars, 100 μm. (B) Levels of osteocalcin, BMPRIA, and BMPRII mRNAs, as determined by semiquantitative RT-PCRs with empty vector-transfected cells and clones 31 and 40 stimulated for 48 h with or without BMP-2. GAPDH mRNA was used as a control for the RNA preparations. (C) Protein levels of BMPRIA and BMPRII in empty vector-transfected cells and clones 31 and 40 stimulated for 48 h with or without BMP-2.

actinomycin D in the presence or absence of BMP-2, there was no difference in the rate of disappearance of the Cdk6 transcript between the treatment and nontreatment groups (Fig. 2B).

Cdk4 is known to be degraded by the ubiquitin-proteasome system (27). Because Cdk6 and Cdk4 are siblings and execute similar functions, we assumed that Cdk6 was likely to be degraded by the same proteolytic system. When MC3T3-E1 cells were treated with MG132, a potent inhibitor of this proteolytic system, during serum stimulation in the absence of BMP-2, the level of Cdk6 was elevated two- to threefold, consistent with this assumption (Fig. 2C). In the presence of BMP-2, MG132 treatment elevated the level of Cdk6 by the same degree, suggesting that there is no acceleration of Cdk6 degradation by treatment with this differentiation inducer. To further confirm that BMP-2 did not affect the stability of the Cdk6 protein, we constructed and analyzed MC3T3-E1 cell clones that constitutively expressed Cdk6 at low and high levels. BMP-2 treatment did not influence the levels of Cdk6 protein expressed from the constitutive EF1α promoter (Fig. 2D). These findings indicate that BMP-2 down-regulates Cdk6 expression mainly, if not exclusively, by transcriptional repression.

Smads mediate BMP-2-induced down-regulation of Cdk6. A differentiation signal invoked by BMP-2 is known to be mediated by Smad proteins, particularly R-Smads and Co-Smads, while I-Smads, such as Smad6 and Smad7, inhibit this signaling (6). To investigate whether Smads mediate Cdk6 down-regulation, we overexpressed Smad6 in MC3T3-E1 cells by use of an adenovirus vector and examined its effect on BMP-2-led Cdk6 down-regulation. As shown in Fig. 3, BMP-2-led Cdk6 down-regulation was completely abolished by the overexpression of Smad6, indicating that Smads do indeed mediate the BMP-2-led Cdk6 down-regulation.

Osteoblasts overexpressing Cdk6 strongly resist BMP-2-invoked differentiation. As discussed above, Cdk6 was down-regulated during BMP-2-invoked osteoblast differentiation. Consequently, a key question is whether this down-regulation is essential for osteoblast differentiation or not. To address this question, we constructed >100 MC3T3-E1 cell clones that stably expressed various levels of Cdk6 by transfecting MC3T3-E1 cells with an expression vector harboring *Cdk6* cDNAs and then tested their ability to respond to BMP-2 and to differentiate into mature osteoblasts. Figure 2D shows the protein levels of Cdk6, Cdk4, and Cdk2 in some representative clones that were treated with BMP-2 or were left untreated compared to the protein levels in similarly treated empty vector-transfected control MC3T3-E1 cells. The Cdk4 and Cdk2 protein levels were not affected by the overexpression of Cdk6, suggesting the absence of any particular compensatory regulation of Cdk4 or Cdk2 expression upon Cdk6 overexpression.

The ability of BMP-2 to induce osteoblast differentiation, as monitored by ALP production and osteocalcin expression, which are well-characterized early and late differentiation markers, respectively, was then studied with control cells and low (~2-fold) and high (>10-fold) Cdk6 expressers. The induction of ALP upon BMP-2 treatment was inhibited significantly in the low expressers and completely in the high expressers (Fig. 4A). Osteocalcin mRNA, as measured by semiquantitative RT-PCR, was markedly reduced in the low expressers and was undetectable in the high expressers (Fig. 4B). Thus, a twofold overexpression of Cdk6, or the same level of exogenous Cdk6 expression as endogenous expression, already showed a strong inhibitory effect on differentiation. This implies that the presence of the original level of Cdk6 expression was enough to markedly inhibit the BMP-2-invoked differentiation of MC3T3-E1 cells.

TABLE 1. Proliferation and cell cycle distribution of MC3T3-E1 cells that overexpress Cdk6[a]

Cell type	BrdU incorporation (OD) at indicated time (h) in presence or absence of BMP-2				Flow cytometric analysis result in presence or absence of BMP-2			
	24		72		% G_0/G_1		%G_2/M	
	−	+	−	+	−	+	−	+
Empty vector	0.37 ± 0.01	0.37 ± 0.12	0.07 ± 0.01	0.08 ± 0.01	78 ± 0	80 ± 1	16 ± 1	15 ± 0
Low expresser	0.41 ± 0.05	0.37 ± 0.08	0.06 ± 0.02	0.08 ± 0.02	78 ± 1	76 ± 0	17 ± 1	18 ± 1
High expresser	0.55 ± 0.07	0.43 ± 0.07	0.05 ± 0.01	0.06 ± 0.01	77 ± 0	79 ± 1	15 ± 1	15 ± 1

[a] Cell proliferation was determined by BrdU incorporation after 24 and 72 h of culture in the presence and absence of BMP-2. Cell cycle distribution was determined by flow cytometric analysis of cells after 24 h of culture. Three representative clones (31, 57, and 75 and 5, 37, and 40, respectively) were chosen from the low- and high-expressing group. Data are expressed as means ± standard deviations after analysis of cells in eight separate wells for each clone.

The Cdk6-led resistance to osteoblast differentiation is unlikely to be caused by an unexpected interference of the BMP-2/Smads signaling pathway by the overexpressed Cdk6. Neither the mRNA nor the protein levels of the BMP receptors BMPRIA and BMPRII were significantly affected by Cdk6 expression (Fig. 4B and C).

Overexpression of Cdk6 does not influence proliferation of osteoblasts. Because Cdk6 promotes the G_1-S transition, the suppression of osteoblast differentiation by overexpressed Cdk6 could be a mere consequence of its execution of this role. We therefore examined the effects of both BMP-2 and Cdk6 overexpression on the G_1-S transition and the proliferation of MC3T3-E1 cells. Empty vector-transfected MC3T3-E1 cells, as well as the low and high Cdk6 expressers, were similarly arrested in quiescence, stimulated with serum in the presence or absence of BMP-2, and analyzed for S-phase entry as well as for cell populations in G_0-G_1 and G_2-M by BrdU incorporation and flow cytometric analyses (Table 1). Cell proliferation was also monitored in the presence and absence of BMP-2 by an XTT assay (Fig. 5). The overexpression of Cdk6 did not cause any significant changes in either the cell cycle distribution or the proliferation rate of the cells, regardless of whether the cells were stimulated with BMP-2 or not. These results suggest that the inhibitory effect of Cdk6 on osteoblast differentiation is not exerted via cell cycle regulation.

The Cdk6-exerted differentiation block is correlated with a loss of the binding of Runx2/Cbfa1, but not Rb, to the osteocalcin promoter. Rb, a potent repressor of the E2F-DP transcriptional factor that is essential for the onset of S phase, has been reported to also act as a transcriptional coactivator for Runx2/Cbfa1, a key transcriptional factor for osteoblast differentiation (23). Since Rb is a direct target of Cdk6 for cell cycle control, we examined whether Rb mediates the Cdk6-exerted inhibition of osteoblastic differentiation by determining the effects of overexpressed Cdk6 on the vivo binding of Runx2/Cbfa1 and Rb to the osteocalcin promoter during BMP-2 treatment. To this end, we performed a ChIP assay. The specificities of the anti-Runx2/Cbfa1 and anti-Rb antibodies used for this assay were confirmed by the lack of precipitation of the irrelevant myogenin promoter, but the clear precipitation of the osteocalcin promoter, by both antibodies (Fig. 6).

Using these antibodies, we compared the binding levels of Runx2/Cbfa1 and Rb to the osteocalcin promoter in empty vector-transfected MC3T3-E1 cells and in low and high Cdk6 expressers at day 1 (a time just after the differentiation commitment) and day 4 (well after the onset of full differentiation phenotypes for MC3T3-E1 cells) post-BMP-2 treatment. As shown in Fig. 6A, on day 1 Runx2/Cbfa1 bound slightly to the osteocalcin promoter in the empty vector-transfected MC3T3-E1 cells, but not in either the low or high Cdk6 expressers, whereas no binding of Rb to this promoter was detected in any of these cells. On day 4, when osteocalcin was fully expressed, the binding of Runx2/Cbfa1 to this promoter was clearly detected in the empty vector-transfected MC3T3-E1 cells and the low Cdk6 expresser, but not in the high Cdk6 expresser, in which osteoblast differentiation was completely blocked (Fig. 4) despite a high level of Runx2/Cbfa1 expression (Fig. 6B). Thus, there was a close correlation between osteoblast differentiation and the binding of Runx2/Cbfa1 to the osteocalcin promoter in Cdk6-led differentiation inhibition. In

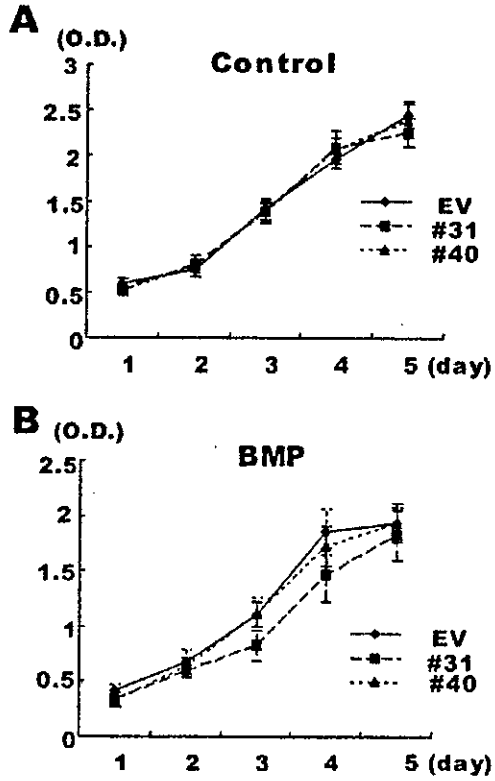

FIG. 5. Overexpression of Cdk6 does not influence proliferation of MC3T3-E1 cells. Proliferation rates were determined by XTT staining of empty vector-transfected cells (EV) and clones 31 and 40 cultured in the presence (B) or absence (A) of BMP-2, with cell sampling done every day.

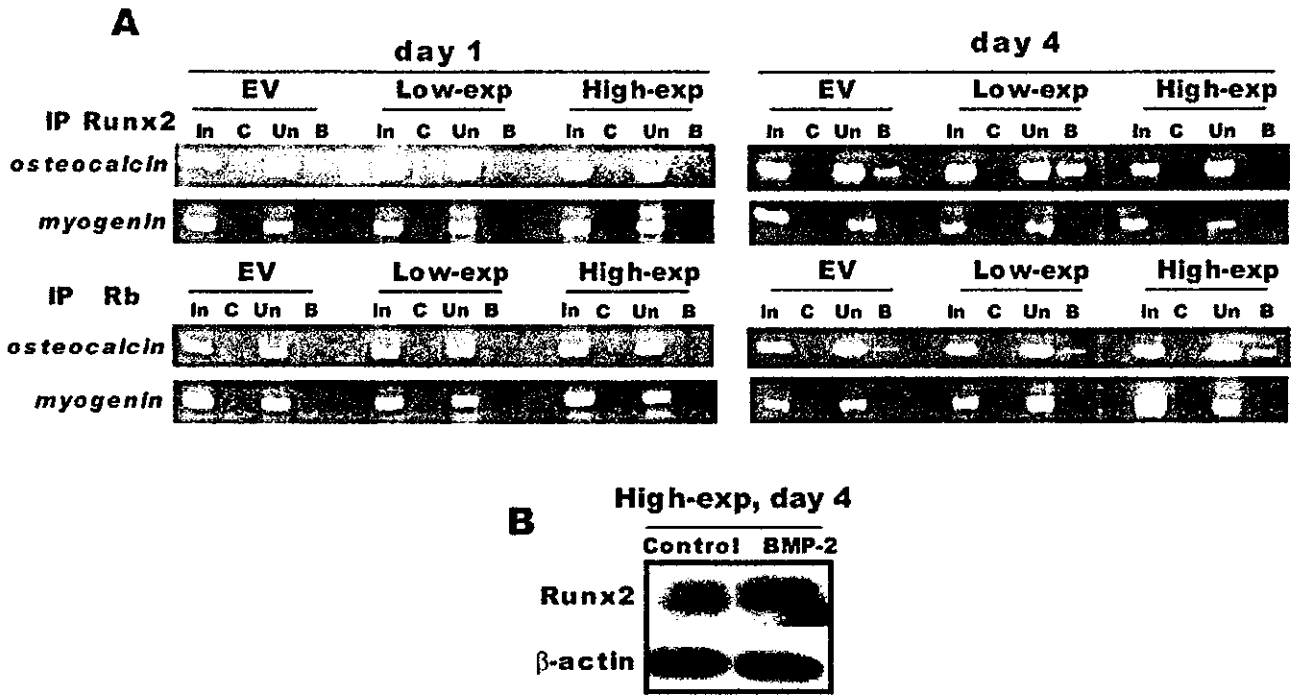

FIG. 6. Cdk6-exerted differentiation block is correlated with a loss of binding of Runx2/Cbfa1, but not Rb, to the osteocalcin promoter. (A) ChIP assay performed with empty vector-transfected MC3T3-E1 cells (EV) and clones 31 (low Cdk6 expresser) and 40 (high Cdk6 expresser) cultured for 1 and 4 days with BMP-2, as described in Materials and Methods. IP Rb, immunoprecipitation with an anti-Rb antibody; IP Runx2, immunoprecipitation with an anti-Runx2/Cbfa1 antibody; In, total DNA input for each sample; C, immunoprecipitation with control serum; Un, PCR from the supernatant after immunoprecipitation; B, PCR from immunoprecipitation product. The primer sets for PCRs of the osteocalcin and myogenin promoter regions are described in Materials and Methods. (B) Runx2/Cbfa1 is expressed in a high Cdk6 expresser cultured for 4 days with or without BMP-2. The level of Runx2/Cbfa1 was determined by Western blotting. The loading control is β-actin.

contrast, there was no apparent correlation between Rb binding and osteoblastic differentiation. On day 4, the binding of Rb to the osteocalcin promoter was detected, as reported previously (23), but it was present in all of the cells, despite the fact that osteoblastic differentiation in the high Cdk6 expresser was completely blocked. Moreover, Rb seemed to bind the promoter independently of Runx2/Cbfa1, because in the high Cdk6 expresser, Rb bound the promoter without the binding of Runx2/Cbfa1.

These ChIP assay results indicate that Rb is unlikely to mediate the Cdk6-led differentiation inhibition, although it is certainly required for the efficient osteoblast differentiation of MC3T3-E1 cells (23). In addition, the loss of Runx2/Cbfa1 binding to the osteocalcin promoter during Cdk6-exerted differentiation inhibition raises the possibility that Cdk6 may inhibit osteoblastic differentiation by blocking the promoter-binding ability of the Runx2/Cbfa1 transcriptional factor.

DISCUSSION

In the present study, we have shown that Cdk6 expression is shut down mainly at transcription upon BMP-2 treatment and that this shutdown, mediated by BMP-2-activated Smad signaling, is required for efficient osteoblast differentiation. Osteoblastic cells, including the presently used MC3T3-E1 cell line and primary mouse osteoblasts, express both Cdk4 and Cdk6, yet only Cdk6 is critically involved in the commitment to dif-

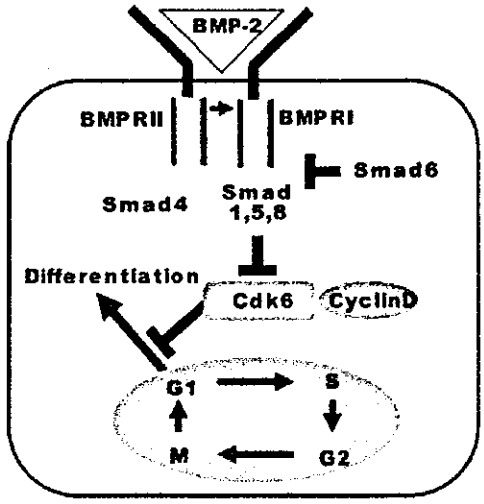

FIG. 7. Schematic presentation of the mechanism by which Cdk6 inhibits osteoblastic differentiation. BMP-2 binds the type II receptor, which subsequently activates the type I receptor by direct association. The activated type I receptor directly phosphorylates R-Smads (Smads 1, 5, and 8) and promotes their complex formation with Co-Smad (Smad4). The R-Smads/Co-Smad complexes are then translocated into the nucleus, where they repress the transcription of the *cdk6* gene and permit osteoblastic differentiation to take place.

ferentiation. This study demonstrates that Cdk6 is a key molecule determining the differentiation rate of osteoblasts as a downstream effector of BMP-2/Smad signaling. Figure 7 depicts a schematic presentation of the mechanism by which BMP-2 induces osteoblast differentiation, as revealed by the present and previous studies. BMP-2 binds to the type II receptor and activates the type I receptor, leading to the formation of R-Smads/Co-Smad complexes, which are imported into the nucleus. The R-Smads/Co-Smad complexes then repress the *cdk6* promoter, thereby removing Cdk6-exerted blocking of differentiation.

The Cdk6-cyclin D3 complex is unique among cyclin D-cognate kinase combinations and evades inhibition by CKIs (8). Therefore, it can greatly enhance the proliferative potential of fibroblasts under growth-suppressive conditions and consequently sensitizes cells to physical and chemical transformation (2). This unique ability of Cdk6, however, does not seem to be responsible for the requirement of Cdk6 down-regulation for efficient osteoblast differentiation because we did not find any noticeable effect of BMP-2 and Cdk6 overexpression on the proliferation or even the cell cycle progression of MC3T3-E1 cells under the experimental conditions we employed. This apparent lack of a growth-stimulating function for Cdk6 in this cell line is consistent with the observation that Cdk4, but not Cdk6, was up-regulated by FGF-2, a potent stimulator of osteoblast proliferation.

The Rb protein has been implicated in osteoblast differentiation. The incidence of osteosarcoma increases 500-fold in patients inheriting *Rb* gene mutations. Recently, the Rb protein was reported to physically interact with Runx2/Cbfa1, which transactivates osteoblast-specific promoters (23). This transactivation is lost in tumor-derived Rb protein mutants, underscoring its potential role in osteoblast differentiation. The possibility that Rb directly mediates the role of Cdk6 as a differentiation inhibitor, however, is remote because unlike for Runx2/Cbfa1, there was no apparent correlation between the Cdk6-exerted differentiation block and the binding of Rb to the osteocalcin promoter.

How could Cdk6 control differentiation without influencing cell cycling? One possibility is that Cdk6 directly controls a factor(s) that is critically involved in differentiation. This possibility may not be as remote as is generally thought. In *Schizosaccharomyces pombe*, Pas1 cyclin and its partner kinase Pef1 activate a transcriptional factor complex that is functionally equivalent to E2F-DP of mammals, thereby promoting S-phase entry, just like Cdk6, yet they independently inhibit mating pheromone signaling, whose activation is essential for the differentiation of yeast cells (22). Thus, this may be a good model for the situation of Cdk6 in BMP-2-induced osteoblast differentiation, highlighting a potential functional similarity between Cdk6 and Pef1.

This study demonstrates for the first time that Cdk6, a G_1 cell cycle factor, plays a critical role in controlling BMP-2-invoked osteoblast differentiation. Several transcription factors, such as Runx2/Cbfa1, osterix, and low-density lipoprotein receptor protein 5, have been reported to be involved in bone formation (12, 16). Consequently, one of these factors may be responsible for the BMP-2-invoked repression of Cdk6 transcription. The identification of the transcriptional repressor as well as key targets of Cdk6 will definitely be required for a deeper understanding of the molecular basis of bone formation.

Finally, it is appropriate to stress that our finding is not specific to BMP-2-induced osteoblast differentiation. Very recently, Matushansky et al. reported a similar role for Cdk6 in the erythroid differentiation of a murine leukemia cell line (10).

ACKNOWLEDGMENTS

We thank Kohei Miyazono and Takeshi Imamura for kindly providing an adenovirus vector carrying *smad6* and Izumu Saito for an adenovirus vector carrying *lacZ*. We also thank H. Chikuda, M. Tsuji, and K. Baba for helpful discussion and support.

This work was supported by grants from the Department of Science, Education and Culture of Japan.

REFERENCES

1. **Bai, S., X. Shi, X. Yang, and X. Cao.** 2000. Smad6 as a transcriptional corepressor. J. Biol. Chem. 275:8267–8270.
2. **Chen, Q., J. Lin, S. Jinno, and H. Okayama.** 2003. Overexpression of Cdk6-cyclin D3 highly sensitizes cells to physical and chemical transformation. Oncogene 22:992–1001.
3. **Deng, C., P. Zhang, J. W. Harper, S. J. Elledge, and P. Leder.** 1995. Mice lacking p21CIP1/WAF1 undergo normal development, but are defective in G1 checkpoint control. Cell 82:675–684.
4. **DiChiara, M. R., J. M. Kiely, M. A. Gimbrone, Jr., M. E. Lee, M. A. Perrella, and J. N. Topper.** 2000. Inhibition of E-selectin gene expression by transforming growth factor beta in endothelial cells involves coactivator integration of Smad and nuclear factor kappaB-mediated signals. J. Exp. Med. 192:695–704.
5. **Hinds, P. W., and R. A. Weinberg.** 1994. Tumor suppressor genes. Curr. Opin. Genet. Dev. 4:135–141.
6. **Kretzschmar, M., and J. Massague.** 1998. SMADs: mediators and regulators of TGF-beta signaling. Curr. Opin. Genet. Dev. 8:103–111.
7. **Lee, K. S., H. J. Kim, Q. L. Li, X. Z. Chi, C. Ueta, T. Komori, J. M. Wozney, E. G. Kim, J. Y. Choi, H. M. Ryoo, and S. C. Bae.** 2000. Runx2 is a common target of transforming growth factor beta1 and bone morphogenetic protein 2, and cooperation between Runx2 and Smad5 induces osteoblast-specific gene expression in the pluripotent mesenchymal precursor cell line C2C12. Mol. Cell. Biol. 20:8783–8792.
8. **Lin, J., S. Jinno, and H. Okayama.** 2001. Cdk6-cyclin D3 complex evades inhibition by inhibitor proteins and uniquely controls cell's proliferation competence. Oncogene 20:2000–2009.
9. **Lopez-Rovira, T., E. Chalaux, J. L. Rosa, R. Bartrons, and F. Ventura.** 2000. Interaction and functional cooperation of NF-kappa B with Smads. Transcriptional regulation of the JunB promoter. J. Biol. Chem. 275:28937–28946.
10. **Matushansky, I., F. Radparvar, and A. I. Skoultchi.** 2003. CDK6 blocks differentiation: coupling cell proliferation to the block to differentiation in leukemic cells. Oncogene 22:4143–4149.
11. **Meyerson, M., G. H. Enders, C. L. Wu, L. K. Su, C. Gorka, C. Nelson, E. Harlow, and L. H. Tsai.** 1992. A family of human cdc2-related protein kinases. EMBO J. 11:2909–2917.
12. **Nakashima, K., X. Zhou, G. Kunkel, Z. Zhang, J. M. Deng, R. R. Behringer, and B. de Crombrugghe.** 2002. The novel zinc finger-containing transcription factor osterix is required for osteoblast differentiation and bone formation. Cell 108:17–29.
13. **Nakayama, K., N. Ishida, M. Shirane, A. Inomata, T. Inoue, N. Shishido, I. Horii, and D. Y. Loh.** 1996. Mice lacking p27(Kip1) display increased body size, multiple organ hyperplasia, retinal dysplasia, and pituitary tumors. Cell 85:707–720.
14. **Nevins, J. R.** 1992. E2F: a link between the Rb tumor suppressor protein and viral oncoproteins. Science 258:424–429.
15. **Nishimori, S., Y. Tanaka, T. Chiba, M. Fujii, T. Imamura, K. Miyazono, T. Ogasawara, H. Kawaguchi, T. Igarashi, T. Fujita, K. Tanaka, and H. Toyoshima.** 2001. Smad-mediated transcription is required for transforming growth factor-beta 1-induced p57(Kip2) proteolysis in osteoblastic cells. J. Biol. Chem. 276:10700–10705.
16. **Patel, M. S., and G. Karsenty.** 2002. Regulation of bone formation and vision by LRP5. N. Engl. J. Med. 346:1572–1574.
17. **Reddi, A. H.** 1998. Role of morphogenetic proteins in skeletal tissue engineering and regeneration. Nat. Biotechnol. 16:247–252.
18. **Sherr, C. J.** 1994. G1 phase progression: cycling on cue. Cell 79:551–555.
19. **Sherr, C. J., and J. M. Roberts.** 1999. CDK inhibitors: positive and negative regulators of G1-phase progression. Genes Dev. 13:1501–1512.
20. **Shi, X., X. Yang, D. Chen, Z. Chang, and X. Cao.** 1999. Smad1 interacts with homeobox DNA-binding proteins in bone morphogenetic protein signaling. J. Biol. Chem. 274:13711–13717.

21. **Takeda, K., H. Ichijo, M. Fujii, Y. Mochida, M. Saitoh, H. Nishitoh, T. K. Sampath, and K. Miyazono.** 1998. Identification of a novel bone morphogenetic protein-responsive gene that may function as a noncoding RNA. J. Biol. Chem. 273:17079–17085.
22. **Tanaka, K., and H. Okayama.** 2000. A Pcl-like cyclin activates the Res2p-Cdc10p cell cycle "start" transcriptional factor complex in fission yeast. Mol. Biol. Cell 11:2845–2862.
23. **Thomas, D. M., S. A. Carty, D. M. Piscopo, J. S. Lee, W. F. Wang, W. C. Forrester, and P. W. Hinds.** 2001. The retinoblastoma protein acts as a transcriptional coactivator required for osteogenic differentiation. Mol. Cell 8:303–316.
24. **Urano, T., H. Yashiroda, M. Muraoka, K. Tanaka, T. Hosoi, S. Inoue, Y. Ouchi, and H. Toyoshima.** 1999. p57(Kip2) is degraded through the proteasome in osteoblasts stimulated to proliferation by transforming growth factor beta1. J. Biol. Chem. 274:12197–12200.
25. **Verschueren, K., J. E. Remacle, C. Collart, H. Kraft, B. S. Baker, P. Tylzanowski, L. Nelles, G. Wuytens, M. T. Su, R. Bodmer, J. C. Smith, and D. Huylebroeck.** 1999. SIP1, a novel zinc finger/homeodomain repressor, interacts with Smad proteins and binds to 5′-CACCT sequences in candidate target genes. J. Biol. Chem. 274:20489–20498.
26. **Vidal, A., and A. Koff.** 2000. Cell-cycle inhibitors: three families united by a common cause. Gene 247:1–15.
27. **Wang, H., T. Goode, P. Iakova, J. H. Albrecht, and N. A. Timchenko.** 2002. C/EBPalpha triggers proteasome-dependent degradation of cdk4 during growth arrest. EMBO J. 21:930–941.
28. **Yan, Y., J. Frisen, M. H. Lee, J. Massague, and M. Barbacid.** 1997. Ablation of the CDK inhibitor p57Kip2 results in increased apoptosis and delayed differentiation during mouse development. Genes Dev. 11:973–983.
29. **Yoshida, Y., S. Tanaka, H. Umemori, O. Minowa, M. Usui, N. Ikematsu, E. Hosoda, T. Imamura, J. Kuno, T. Yamashita, K. Miyazono, M. Noda, T. Noda, and T. Yamamoto.** 2000. Negative regulation of BMP/Smad signaling by Tob in osteoblasts. Cell 103:1085–1097.
30. **Zhang, P., N. J. Liegeois, C. Wong, M. Finegold, H. Hou, J. C. Thompson, A. Silverman, J. W. Harper, R. A. DePinho, and S. J. Elledge.** 1997. Altered cell differentiation and proliferation in mice lacking p57KIP2 indicates a role in Beckwith-Wiedemann syndrome. Nature 387:151–158.
31. **Zhang, Y. W., N. Yasui, K. Ito, G. Huang, M. Fujii, J. Hanai, H. Nogami, T. Ochi, K. Miyazono, and Y. Ito.** 2000. A RUNX2/PEBP2alphaA/CBFA1 mutation displaying impaired transactivation and Smad interaction in cleidocranial dysplasia. Proc. Natl. Acad. Sci. USA 97:10549–10554.
32. **Zhu, H., P. Kavsak, S. Abdollah, J. L. Wrana, and G. H. Thomsen.** 1999. A SMAD ubiquitin ligase targets the BMP pathway and affects embryonic pattern formation. Nature 400:687–693.
33. **Zimmermann, M.** 1983. Ethical guidelines for investigations of experimental pain in conscious animals. Pain 16:109–110.BM

Available online at www.sciencedirect.com
SCIENCE DIRECT®
Biomaterials 26 (2005) 1381–1388
Biomaterials
www.elsevier.com/locate/biomaterials

Photo-immobilization of a phospholipid polymer for surface modification

Tomohiro Konno[a,b], Hirokazu Hasuda[a], Kazuhiko Ishihara[b], Yoshihiro Ito[a,*]

[a] *Regenerative Medical Bioreactor Project, Kanagawa Academy of Science and Technology, KSP East 309, 3-2-1 Sakado, Takatsu-ku, Kawasaki, Kanagawa 213-0012, Japan*

[b] *Department of Materials Engineering, Graduate School of Engineering, The University of Tokyo, 7-3-1, Hongo, Bunkyo-ku, Tokyo 113-8656, Japan*

Received 27 December 2003; accepted 30 April 2004

Available online 19 June 2004

Abstract

A photo-reactive polymer having a phospholipid polar group was prepared, and the polymer was photo-immobilized on polymeric surfaces, where its interactions with biocomponents were investigated. By using a photo-immobilization method, the polymer was used for surface modification of polyethylene and polypropylene, polymers whose surfaces were not treated in our previous development of the phosphorylcholine-derived polymer. The photo-reactive polymer was synthesized by a coupling reaction involving copolymer consisting of 2-methacryloyloxyethyl phosphorylcholine and methacrylic acid with 4-azidoaniline. When the polymer was unpattern immobilized on the surface, X-ray photo-electron spectroscopic analysis and static contact angle measurements were performed. It was shown that the surface was covered with phospholipid polar groups. Micropattern immobilization was carried out using a micropatterned photo-mask. Measurements using atomic force microscopy showed that the swelled micropatterned polymer was five times as thick as the dried one. Protein adsorption and platelet adhesion were reduced on the polymer-immobilized regions. Mammalian cells did not adhere, and formed aggregates on the immobilized regions. In conclusion, the photo-reactive phospholipid polymer was covalently immobilized on the conventional polymer surfaces and it tended to reduce interactions with proteins and cells.

Keywords: Photo-immobilization; Phospholipid polymer; Surface modification; Protein adsorption; Cell adhesion

1. Introduction

Lipid membranes are used as biomimetic systems, and are expected to become a key component of novel biomolecular materials [1–14]. In particular, lipid bilayer membranes on solid supports have been the subject of numerous publications [1–11]. The membranes prepared on various solids by optimized variations of the available deposition chemistries have been shown to accommodate a variety of proteins and enzymes in controlled orientations and in active conformations. The supported lipid bilayer is considered to mimic the native environment of membrane-associated biomolecules. These membranes are also promising surfaces for developing new biosensors and coating materials that resist non-specific interactions with proteins and cells.

The lipid head group of phosphorylcholine, a zwitterion, is a common group in the lipid molecules that form biological membranes, and is considered to play an important role as a surface material for biomedical devices by reducing interaction with proteins and cells. As a biomimetic polymer, 2-methacryloyloxyethyl phosphorylcholine (MPC)-containing polymer was synthesized by the group of Ishihara and Nakabayashi [15,16]. The polymer shows non-thrombogenicity, that is, suppression of non-specific protein adsorption, platelet adhesion, activation, and aggregation when the polymer contacted whole blood, even in the absence of anticoagulants.

Recently, some types of MPC-containing copolymers have been synthesized for coating [17] and covalent immobilization was achieved [18–20]. However, the

*Corresponding author. Tel.: +81-44-819-2044; fax: +81-44-819-2039.

E-mail address: y-ito@ksp.or.jp (Y. Ito).

0142-9612/$ - see front matter © 2004 Elsevier Ltd. All rights reserved.
doi:10.1016/j.biomaterials.2004.04.047

covalent immobilization was limited to specialized surfaces. Therefore, in the present investigation, photo-immobilization was employed for covalent immobilization of the polymer on a broader variety of surfaces.

In addition, although many synthetic polymers have been devised to improve surface reducing interaction with proteins or cells, it is difficult to directly compare the surface properties of different polymers under precisely the same conditions. Therefore, a micropatterning method has been devised for lipids and polymers [21–23], and the method has proved useful for comparing the interaction of polymers with proteins and cells [24–26]. We modified the method of Matsuda and Sugawara [27], and have applied this method to some growth factors [28–30], sulfated hyaluronic acid [31], heparin [32], and thermo-responsive polymer [33]. In the present study, micropatterning of MPC polymer was performed, and the interactions with proteins and cells were investigated.

2. Materials and methods

2.1. Synthesis of photo-reactive MPC polymer

The polymer synthesis is illustrated in Fig. 1. MPC copolymer consisting of MPC (90 mol%) and methacrylic acid (10 mol%) was obtained from NOF Co. Ltd. (Tokyo, Japan), and is referred to as PMAc. The molecular weight of PMAc, as measured by gel permeation chromatography, was 2.2×10^5. Modification of PMAc was performed as follows: 4-azidoaniline (12.44 mg) and water-soluble carbodiimide (17.47 mg) were dissolved in 2 ml of PMAc solution (5 wt%) and 98 ml of water was added to the solution. The solution was left to stand for 24 h. After the reaction, the product was dialyzed with dialysis cassette (PIERCE, Rockford, IL) until no further release of azidoaniline through the cassette was confirmed by ultraviolet (UV) absorption. The resultant solution was freeze-dried. The azidophenyl-derivatized PMAc is referred to as Az-PMAc. Elemental analysis indicated that the amount of azidophenyl group in Az-PMAc was 6%.

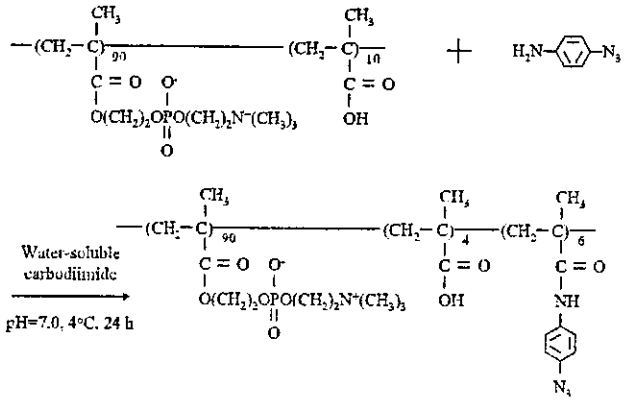

Fig. 1. Synthetic scheme for photo-reactive phosphorylcholine-containing polymer.

2.2. Micropatterning

The micropatterning method is illustrated in Fig. 2. An aqueous solution of Az-PMAc (1 wt%) was cast on polyethylene and polypropylene plates (diameter 22 mm), which were purchased from Sarstedt (Newton, NC) and from Nikkyo Technos Co. Ltd. (Tokyo, Japan), respectively, and air-dried at room temperature. Subsequently, the plate was covered with a photo-mask, which was manufactured by Toppan Printing Co. Ltd. (Tokyo, Japan) and was UV-irradiated with a UV lamp (UV Spot Light Source L5662, Hamamatsu Photonics, Hamamatsu, Japan) from a distance of 5 cm for 10 s ($16\,mW/cm^2$). When an unpatterned surface was prepared, the photo-mask was not employed. The plate was then repeatedly washed with distilled water.

2.3. Measurement of contact angle

The unpatterned sample was placed on the holder of a CA-W Automatic Contact Angle Meter (Kyowa Interface Science Co. Ltd., Saitama, Japan) and a drop of water (0.4 μl) was put on the sample surface. The contact angle of the drop on the surface was measured at room temperature. At least 10 contact angles on different areas were measured and averaged.

2.4. Measurement by X-ray photo-electron spectroscopy (XPS)

The unpatterned sample was inserted in the holder of an XPS, AXIS-HSi (Shimadzu/Kratos, Kyoto, Japan). After evacuation, the measurement was carried out under 3×10^{-9} Torr. The X-ray source was CuK_α, the applied voltage was 12 kV, and the electric current was

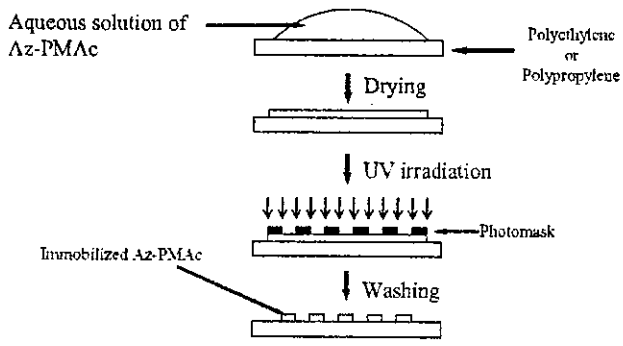

Fig. 2. Schematic illustration of micropatterning procedure.

10 mA. The take-off angle of the photo-electrons was 90°.

2.5. Measurement by atomic force microscopy (AFM)

The measurement was performed using an SPI-3800 (Seiko Instruments Inc., Chiba, Japan). The micropatterned sample was dried in vacuo for 1 day at room temperature and was set in a cell holder into which water could be injected. After observation of the dry sample, distilled water was injected into the sample cell and the same position was observed. The measurement was performed using the tapping mode with a nominal force constant of 0.09 N/m.

2.6. Interaction with proteins

Fluorescein isothiocyanate (FITC)-labeled bovine serum albumin and FITC-labeled immunoglobulin were purchased from Sigma (St. Louis, MO). FITC-labeled fibrinogen was prepared as follows: a phosphate-buffered solution (PBS; 25 ml) containing human fibrinogen (500 μg) was added dropwise to a PBS (25 ml, pH 8.0) containing FITC (12.5 μg) and the pH of the mixture was adjusted to 9.0. The mixture was stirred at room temperature for 2 h. The resulting solution was dialyzed against double-distilled water using a Millipore dialysis tube (cut-off less than 10 000) at 4°C until the release of FITC became undetectable by fluorescence spectroscopy. Finally, the purified protein was lyophilized. All procedures were carried out in darkness.

The protein adsorption experiment was performed as follows: the sample plates were incubated in PBS containing the FITC-labeled albumin (10 mg/ml), FITC-labeled immunoglobulin (2 mg/ml), or the FITC-labeled fibrinogen (10 mg/ml) at 37°C for 10 min. After being washed with PBS, the sample was observed by fluorescence microscopy.

2.7. Interaction with platelets

Human whole blood was collected from healthy volunteers in a disposable syringe containing 3 ml of aqueous solution of 3.8 wt% sodium citrate. The citrated whole blood was immediately centrifuged for 15 min at 1200 rpm to obtain citrated platelet-rich plasma (PRP). The micropatterned sample plates were placed in contact with PRP and left for 60 min at 37°C. The PRP was removed with an aspirator, and the membrane was rinsed three times with PBS. Subsequently, 2.5 vol% glutaraldehyde in PBS was poured into each well containing the sample plates, and the samples were stored at room temperature for 2 h in order to fix the blood components on the sample plate. After it had been rinsed sufficiently with distilled water, the samples were freeze-dried. The surface of the sample plate was observed with a scanning electron microscope (SEM) after gold-sputtering treatment.

2.8. Cell culture

RAW264 (originating from leukemic mouse monocytes) cells were purchased from Riken Cell Bank (Tsukuba, Japan) and were cultured in minimum essential medium (Sigma, St. Louis, MO) with 10% fetal bovine serum and 1% non-essential amino acids (Invitrogen Life Technologies, Carlsbad, CA). The recovered cells were washed with the culture medium and suspended in each medium containing no serum (3×10^5 cells per 60 mm-diameter culture dish). The cell suspension was added to the sample plate, which was sterilized with 70% ethanol. The cells were incubated at 37°C under 5% v/v of CO_2 and were observed by a phase-contrast microscope equipped with a video camera.

3. Results and discussion

3.1. Synthesis of photo-reactive MPC polymer

The UV and fluorescence spectra of Az-PMAc are shown in Fig. 3. In the UV spectrum of the photo-reactive polymer, an absorption at 269 nm, which is assignable to the azidophenyl group, was observed.

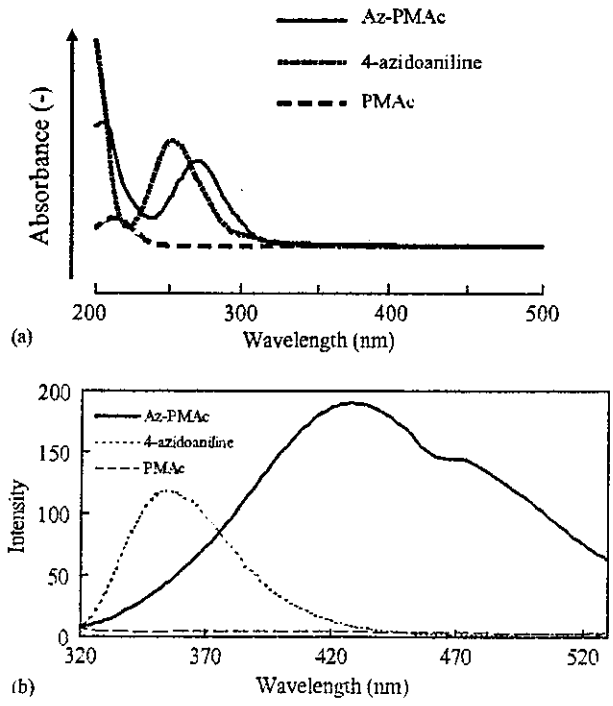

Fig. 3. UV (a) and fluorescence (b) spectra of azidoaniline, PMAc, and Az-PMAc.

Fig. 3a indicates that the absorption was slightly red shifted from the corresponding absorption of 4-azidoaniline, and Fig. 3b shows that the fluorescence was red shifted. These shifts may be due to electron delocalization of the azidophenyl group caused by amide bond formation. In previous studies, the peaks of photo-reactive hyaluronic acid and photo-reactive heparin were also red shifted from 4-azidoaniline [35,37].

3.2. Photo-immobilization

The Az-PMAc was coated on the plates and the coated surface was UV-irradiated with a photo-mask (Fig. 4). The surface pattern was the same as that of the photo-mask. The micropatterned surface was observed by phase-contrast microscopy (Fig. 4b) and by fluorescence microscopy (Fig. 4c). It is known that azido groups are decomposed by UV irradiation, and nitrene groups, which are highly reactive radical groups, are produced. The cast Az-PMAc formed molecular networks as a result of the produced radical groups. In addition, a micropatterned surface was formed both on polyethylene (Fig. 4c) and polypropylene (Fig. 4d) plates. The present result demonstrates that photo-immobilization is useful for covalent immobilization of MPC on various materials.

Previously, Prucker et al. [34] reported photo-chemical attachment of polymer films to solid surfaces via benzophenone derivatives. In their case, the amount of immobilized polymer on the surface reached saturation after about 10–20 min, when the light intensity was 100 mW/cm^2. In the present study, 10 s were enough for preparation of micropatterned immobilization, although the intensity was 16 mW/cm^2. Although the strength of binding of immobilized polymer to the surface has not been investigated, it was demonstrated that 10 s was enough for washing out of non-bound polymers.

The unpatterned PMAc surface on the polyethylene plate was made by UV-irradiation without a photo-mask. XPS measurement of the unpatterned surface demonstrated that the surface was covered with phospholipid polar groups (Fig. 5). In addition to the XPS spectrum of the previously reported MPC polymer coating surface [35,36], a new peak that was ascribed to the amide bond formed by reaction between PMAc and azidoaniline was found at 398 eV.

The water contact angle was measured on the unpatterned surface (Fig. 6). The contact angle on the

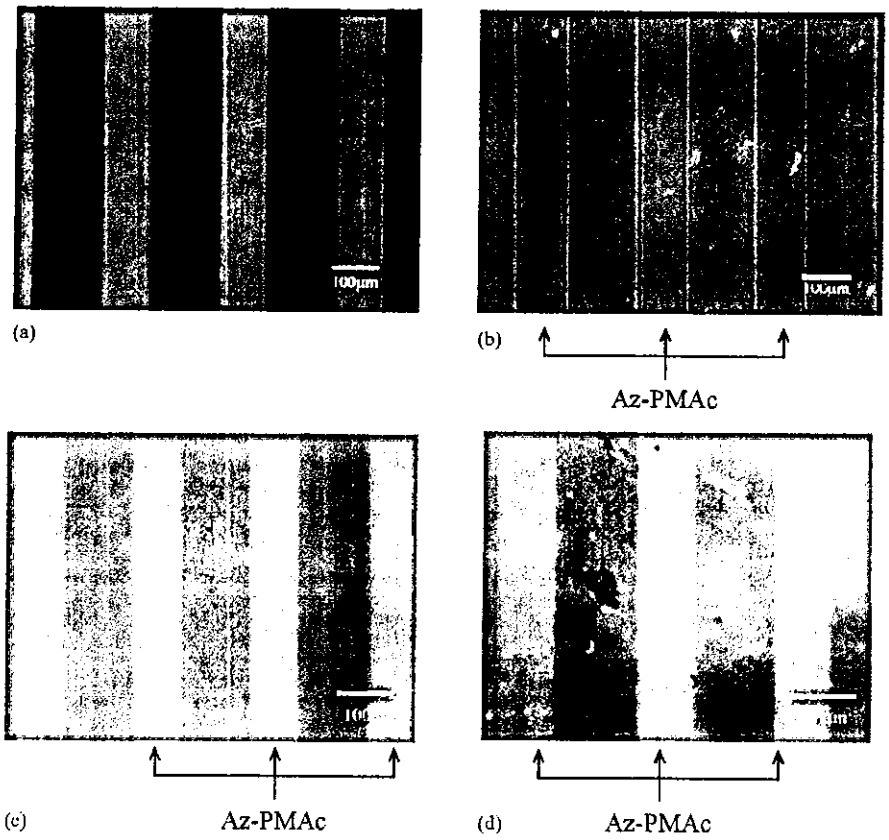

Fig. 4. Phase-contrast micrographs of photo-mask (a); and micropatterned surface of the polyethylene plate (b); fluorescence micrographs of micropatterned surface of the polyethylene plate (c); and of the polypropylene plate (d).

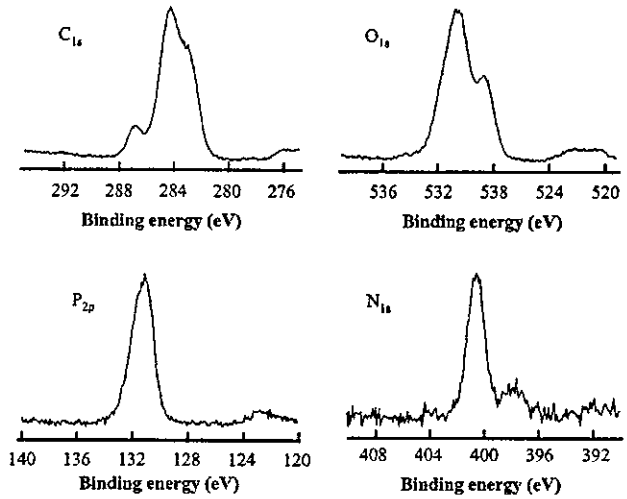

Fig. 5. XPS spectra of the Az-PMAc immobilized polyethylene surface.

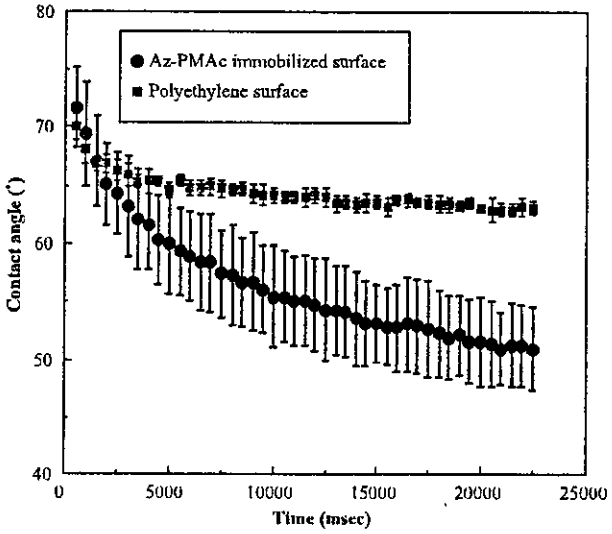

Fig. 6. Time course of static contact angle of water on the Az-PMAc-immobilized and non-immobilized polyethylene surface.

PMAc-immobilized surface rapidly decreased with time, although that on the polyethylene surface did not. It was demonstrated that a hydrophilic surface was formed by immobilization of the PMAc.

The surface was observed by AFM, as shown in Fig. 7. In the dried state, the thickness was about 800 nm. However, the PMAc layer rapidly swelled in water to a thickness of about 4000 nm. The hydrogel state of PMAc was formed after soaking for 10 min in water. Fig. 8 shows the force curves of the micropatterned surface. On the surface of bare polyethylene (2, 4, 6, 8, 10), the force abruptly increased with decreasing distance between the cantilever and the surface. On the other hand, on the Az-PMAc-immobilized region (1, 3,

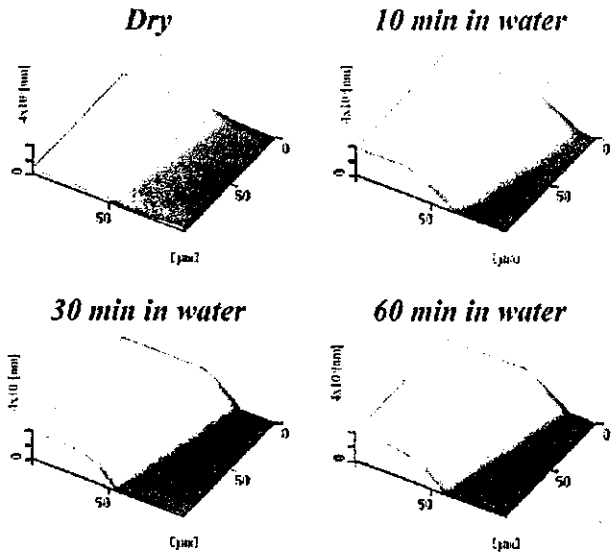

Fig. 7. AFM images of the Az-PMAc-micropatterned surface. The dried sample was measured and then incubated in water for different periods.

5, 7, 9) the force did not increase so abruptly with the decrease of distance. These results demonstrated that the Az-PMAc surface was so soft that force was not significantly produced on the surface.

3.3. Interaction with biological components

The sample plate was immersed in the protein solutions, and the protein-adsorbed sample was observed by fluorescence microscopy (Fig. 9). Albumin, immunoglobulin, and fibrinogen predominantly adsorbed onto the non-immobilized surface. The fluorescence intensity of adsorbed proteins is significantly higher than that of Az-PMAc alone. Previously, we reported that an MPC-adsorbed surface inhibited adsorption of proteins [37,38]. The present study confirmed the previous reports.

Human blood platelet adhesion onto the micropatterned surface was observed by SEM. The number of platelets on the PMAc-immobilized regions $(0.34 \pm 0.02) \times 10^3$ cell/μm^2 was significantly less than that on the non-immobilized regions $(1.13 \pm 0.12) \times 10^3$ cell/μm^2. The non-adhesiveness of MPC polymer has been reported previously [38]. The present study critically demonstrated this property.

The time course of behavior of RAW264 on the micropatterned surface is shown in Fig. 10. When the cells were added to the surface, they randomly distributed independent of the immobilized material. However, after 5 min, they began to aggregate on the Az-PMAc-immobilized surface; the cellular aggregates increased in size with time and eventually floated. On the

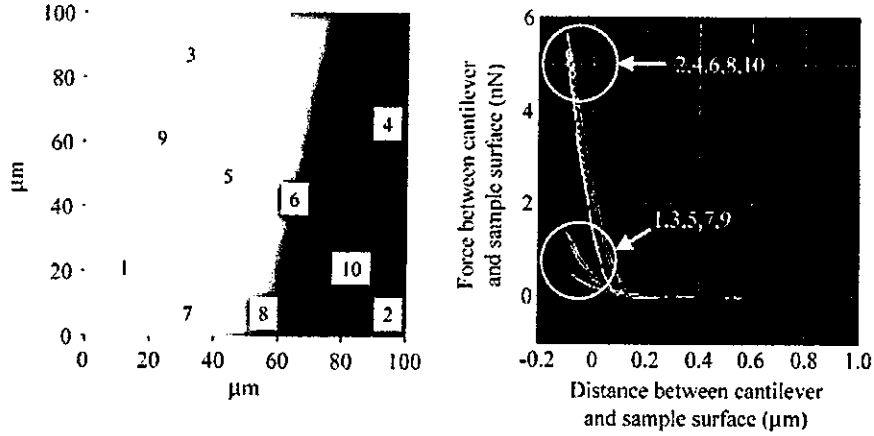

Fig. 8. Contact points of the cantilever with surfaces and the force curve between the cantilever and surfaces. The numbers represent the contact points of the cantilever. Points 1, 3, 5, 7, and 9 were on the Az-PMAc-immobilized surface and points 2, 4, 6, 8, and 10 on the bare polyethylene surface.

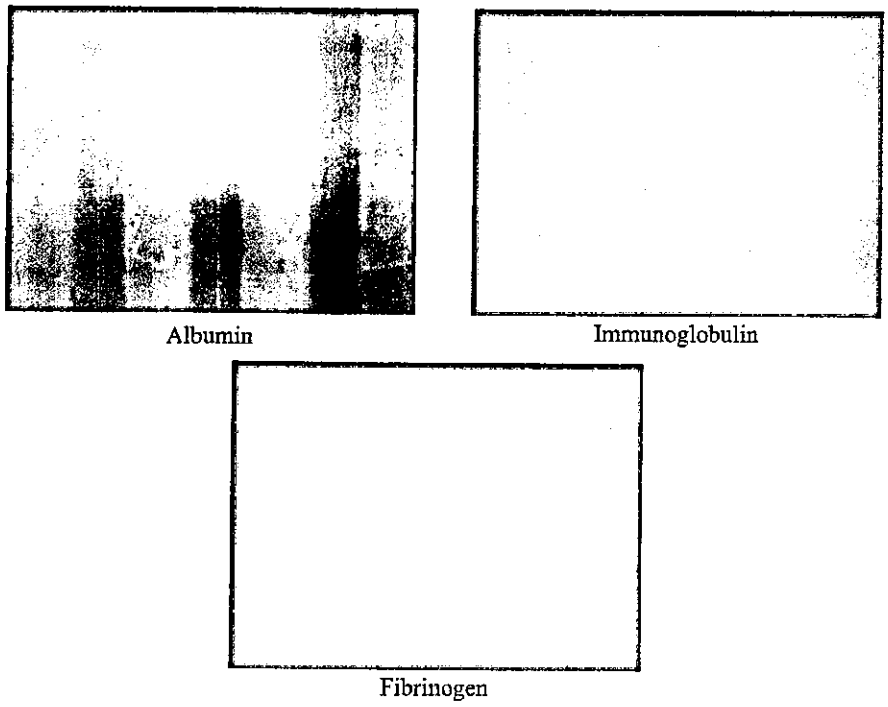

Fig. 9. Fluorescence micrographs of proteins (albumin, immunoglobulin, and fibrinogen) adsorbed onto the Az-PMAc-micropatterned polyethylene surface. The wavelengths of excitation and emission were 470±20 and 525±25 nm, respectively.

non-immobilized region the cells adhered and spread on the surface. The floated aggregates on the Az-PMAc-immobilized region were completely removed by mild shaking. It is known that RAW264 shows macrophage-like properties and tends to adhere to various materials [39]. It was demonstrated that PMAc inhibited the adhesion of even very adhesive cells.

The present study demonstrated photo-immobilization of a phospholipid polymer and visualized the interactions with biocomponents such as proteins, platelets, and cells. The photo-immobilization technique is useful for surface modification and the phospholipid polymer significantly reduced the interactions with proteins and cells.

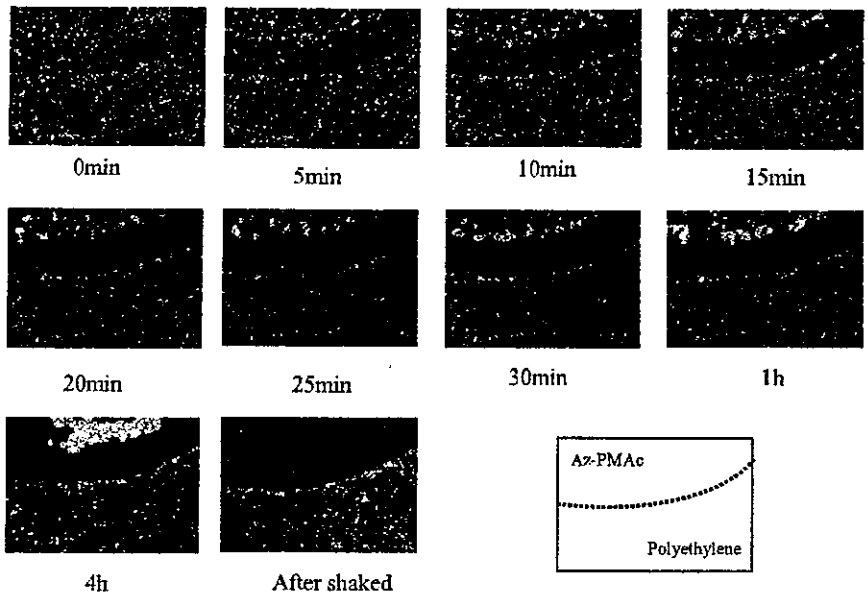

Fig. 10. Time course of behavior of RAW264 cells on Az-PMAc-immobilized and non-immobilized region (polyethylene surface), as observed by phase-contrast microscopy with a video camera.

Acknowledgements

This work was supported in part by a grant from the Japanese Ministry of Education, Culture, Sports, Science, and Technology (14380406). The authors thank Mr. Akihiko Watanabe for his support with the AFM measurement.

References

[1] Shen WW, Boxer SG, Knoll W, Frank C. Polymer-supported lipid bilayers on benzophenone-modified substrates. Biomacromolecules 2001;2:70–9.
[2] Naumann CA, Prucker O, Lehmann T, Rühe J, Knoll W, Frank CW. The polymer-supported phospholipid bilayer: tethering as a new approach to substrate-membrane stabilization. Biomacromolecules 2002;3:27–35.
[3] Mennicke U, Salditt T. Preparation of solid-supported lipid bilayers by spin-coating. Langmuir 2002;18:8172–7.
[4] Devadoss A, Burgess JD. Detection of cholesterol through electron transfer to cholesterol oxidase in electrode-supported lipid bilayer membranes. Langmuir 2002;18:9617–21.
[5] Andersson AS, Glasmästar K, Sutherland D, Lidberg U, Kasemo B. Cell adhesion on supported lipid bilayers. J Biomed Mater Res 2003;64A:622–9.
[6] Richter RP, Brisson A. Characterization of lipid bilayers and protein assemblies supported on rough surfaces by atomic force microscopy. Langmuir 2003;19:1632–40.
[7] Baumgart T, Offenhäuser A. Polysaccharide-supported planar bilayer lipid model membranes. Langmuir 2003;19:1730–7.
[8] Ross EE, Rozanski LJ, Spratt T, Liu S, O'Brien DF, Saavedra SS. Planar supported lipid bilayer polymers formed by vesicle fusion. 1. Influence of diene monomer structure and polymerization method on film properties. Langmuir 2003;19:1752–65.
[9] Sengupta K, Schilling J, Marx S, Fischer M, Bacher A, Sackmann E. Mimicking tissue surfaces by supported membrane coupled ultrathin layer of hyaluronic acid. Langmuir 2003;19:1775–81.
[10] Zhao J, Tamm LK. FTIR and fluorescence studies of interactions of synaptic fusion proteins in polymer-supported bilayers. Langmuir 2003;19:1838–46.
[11] Schneider J, Barger W, Lee GU. Nanometer scale surface properties of supported lipid bilayers measured with hydrophobic and hydrophilic atomic force microscope probes. Langmuir 2003;19:1899–907.
[12] Sun XL, Liu H, Orban JM, Sun L, Chaikof EL. Synthesis and terminal functionalization of a polymerizable phosphatidylethanolamine. Bioconjugate Chem 2001;12:673–7.
[13] Schuster B, Weighert S, Pum D, Sára M, Sleytr UB. New method for generating tetraether lipid membranes on porous supports. Langmuir 2003;19:2392–7.
[14] Elliot JT, Burden DL, Woodward JT, Sehgal A, Douglas JF. Phospholipid monolayers supported on spun cast polystyrene films. Langmuir 2003;19:2275–83.
[15] Ishihara K, Ueda T, Nakabayashi N. Preparation of phospholipids polymers and their properties as polymer hydrogel membrane. Polym J 1990;22:355–60.
[16] Ishihara K, Iwasaki Y. Reduced protein adsorption on novel phospholipids polymers. J Biomater Appl 1998;13:111–27.
[17] Lewis AL, Hughes PD, Kirkwood LC, Leppard SW, Redman RP, Tolhurs LA, Stratford PW. Synthesis and characterization of phosphorylcholine-based polymers useful for coating blood filtration devices. Biomaterials 2000;21:1847–59.
[18] Lewis AL, Cumming ZL, Goreish HH, Kirkwood LC, Tolhurs LA, Stratford PW. Crosslinkable coatings from phosphorylcholine-based polymers. Biomaterials 2001;22:99–111.
[19] Court JL, Redman RP, Wang JH, Leppard SW, O'Byrne VJ, Small SA, Lewis AL, Jones SA, Stratford PW. A novel phosphorylcholine-coated contact lens for extended wear use. Biomaterials 2001;22:3261–72.
[20] Lu JR, Murphy EF, Su TJ, Lewis AL, Stratford PW, Satija SK. Reduced protein adsorption on the surface of a chemically grafted phospholipid monolayer. Langmuir 2001;17:3382–9.

[21] Yoshina-Ishii C, Boxer SG. Arrays of mobile tethered vesicles on supported lipid bilayers. J Am Chem Soc 2003;125:3696–7.
[22] Kam L, Boxer SG. Spatially selective manipulation of supported lipid bilayers by laminar flow: steps toward biomembrane microfluidics. Langmuir 2003;19:1624–31.
[23] Carlson JW, Bayburt T, Sligar SG. Nanopatterning phospholipid bilayers. Langmuir 2000;16:3927–31.
[24] Grooves JT, Mahal LK, Bertozzi CR. Control of cell adhesion and growth with micropatterned supported lipid membranes. Langmuir 2001;17:5129–33.
[25] Orth RN, Wu M, Holowka DA, Craighead HG, Baird BA. Mast cell activation on patterned lipid bilayers of subcellular dimensions. Langmuir 2003;19:1599–605.
[26] Sapuri AR, Baksh MM, Grooves JT. Electrostatically targeted intermembrane lipid exchange with micropatterned supported membranes. Langmuir 2003;19:1606–10.
[27] Matsuda T, Sugawara T. Photochemical protein fixation on polymer surfaces via derivatized phenyl azido group. Langmuir 1995;11:2272–6.
[28] Ito Y. Surface micropatterning to regulate cell functions. Biomaterials 1999;20:2333–42.
[29] Chen G, Ito Y. Gradient micropattern immobilization of EGF to investigate the effect of artificial juxtacrine stimulation. Biomaterials 2001;22:2453–7.
[30] Ito Y, Chen G, Imanishi Y, Morooka T, Nishida E, Okabayashi Y, Kasuga M. Differential control of cellular expression by diffusible and non-diffusible EGF. J Biochem 2001;129:733–7.
[31] Chen G, Ito Y, Imanishi Y, Magnani A, Lamponi S, Barbucci R. Photoimmobilization of sulphated hyaluronic acid for antithrombogenicity. Bioconjugate Chem 1997;8:730–4.
[32] Ito Y, Hayashi M, Imanishi Y. Gradient micropattern immobilization of heparin and its interaction with cells. J Biomater Sci Polym Ed 2001;12:367–78.
[33] Liu H, Ito Y. Gradient-micropattern-immobilization of a thermoresponsive polymer to investigate its effect on cell behaviors. J Biomed Mater Res 2003;67A:1424–9.
[34] Prucker O, Naumann CA, Rühe J, Knoll W, Frank CW. Photochemical attachment of polymer films to solid surfaces via monolayers of benzophenone derivatives. J Am Chem Soc 1999;121:8766–70.
[35] Ishihara K, Tanaka S, Furukawa N, Kurita K, Nakabayashi N. Improved blood compatibility of segmented polyurethanes by polymeric additives having phospholipid polar groups. I. Molecular design of polymeric additives and their functions. J Biomed Mater Res 1996;32:391–9.
[36] Ishihara K, Ishikawa E, Iwasaki Y, Nakabayashi N. Inhibition of fibroblast cell adhesion on substrate by coating with 2-methacryloyloxyethyl phosphorylcholine polymers. J Biomater Sci Polym Ed 1999;10:1047–61.
[37] Iwasaki Y, Fujiike A, Kurita K, Ishihara K, Nakabayashi N. Effect of reduced protein adsorption on platelet adhesion at the phospholipid polymer surfaces. J Biomater Sci Polym Ed 1996;8:151–63.
[38] Iwasaki Y, Ishihara K, Nakabayashi N, Khang G, Jeon JH, Lee JW, Lee HB. Platelet adhesion on the gradient surfaces grafted with phospholipid polymer. J Biomater Sci Polym Ed 1998;9:801–16.
[39] Ito Y, Nogawa M. Preparation of a protein-array using a photoreactive polymer for a cell adhesion assay. Biomaterials 2003;24:3021–6.